NAVAL POSTGRADUATE SCHOOL

MONTEREY, CALIFORNIA

THESIS

PERFORMANCE ANALYSIS OF THE EFFECT OF PULSED-NOISE INTERFERENCE ON WLAN SIGNALS TRANSMITTED OVER A NAKAGAMI FADING CHANNEL

by
Andreas Tsoumanis

March 2004

Thesis Advisor:	R. Clark Robertson
Second Reader:	Donald Wadsworth

THIS PAGE INTENTIONALLY LEFT BLANK

REPORT DOCUMENTATION PAGE		Form Approved OMB No. 0704-0188

Public reporting burden for this collection of information is estimated to average 1 hour per response, including the time for reviewing instruction, searching existing data sources, gathering and maintaining the data needed, and completing and reviewing the collection of information. Send comments regarding this burden estimate or any other aspect of this collection of information, including suggestions for reducing this burden, to Washington headquarters Services, Directorate for Information Operations and Reports, 1215 Jefferson Davis Highway, Suite 1204, Arlington, VA 22202-4302, and to the Office of Management and Budget, Paperwork Reduction Project (0704-0188) Washington DC 20503.

1. AGENCY USE ONLY *(Leave blank)*	**2. REPORT DATE** March 2004	**3. REPORT TYPE AND DATES COVERED** Master's Thesis

4. TITLE AND SUBTITLE: Title (Mix case letters)
Performance Analysis of the Effect of Pulsed-noise Interference on WLAN Signals Transmitted over a Nakagami Fading Channel.

5. FUNDING NUMBERS

6. AUTHOR
Andreas Tsoumanis

7. PERFORMING ORGANIZATION NAME AND ADDRESS
Naval Postgraduate School
Monterey, CA 93943-5000

8. PERFORMING ORGANIZATION REPORT NUMBER

9. SPONSORING /MONITORING AGENCY NAME AND ADDRESS35
N/A

10. SPONSORING/MONITORING AGENCY REPORT NUMBER

11. SUPPLEMENTARY NOTES The views expressed in this thesis are those of the author and do not reflect the official policy or position of the Department of Defense or the U.S. Government.

12a. DISTRIBUTION / AVAILABILITY STATEMENT
Approved for public release; distribution is unlimited.

12b. DISTRIBUTION CODE

13. ABSTRACT (maximum 200 words)

This thesis examines the performance of wireless local area network (WLAN) signals, specifically, the signal of IEEE 802.11a standard. The signal is subject to pulsed-noise jamming, when either the desired signal alone or the desired signal and the jamming signal are subject to Nakagami fading. As expected, the implementation of forward error correction (FEC) coding with soft decision decoding (SDD) and maximum-likelihood detection improves performance as compared to uncoded signals. In addition, the combination of maximum-likelihood detection and error correction coding renders pulsed-noise jamming ineffective as compared to barrage noise jamming. When the jamming signal encounters fading as well, we assume that the average jamming power is much greater than the AWGN power. For uncoded signals, a jamming signal that experiences fading actually improves performance when the parameter of the information signal m_s is less than or equal to one. Surprisingly, for larger values of m_s a jamming signal that experiences fading works in favor of the information signal only for small signal-to-interference ratio (SIR). When SIR is large, performance when the jamming signal experiences fading is worse relative to performance when the jamming signal does not experience fading. For error correction coding with SDD, we investigate only continuous jamming since it is by far the worst-case. Moreover, while we consider a range of fading conditions for the jamming signal, we examine only Rayleigh fading of the information signal. The coded signal, when the jamming signal experiences severe fading, performs better relative to the case when the jamming signal does not experience fading.

14. SUBJECT TERMS IEEE 802.11a, WLAN, FEC, SDD, OFDM, BPSK, QPSK, MQAM, AWGN, Nakagami, soft decision decoding, convolutional code, pulsed-noise jamming, probability of bit error	**15. NUMBER OF PAGES** 87
	16. PRICE CODE

17. SECURITY CLASSIFICATION OF REPORT	**18. SECURITY CLASSIFICATION OF THIS PAGE**	**19. SECURITY CLASSIFICATION OF ABSTRACT**	**20. LIMITATION OF ABSTRACT**
Unclassified	Unclassified	Unclassified	UL

NSN 7540-01-280-5500

Standard Form 298 (Rev. 2-89)
Prescribed by ANSI Std. 239-18

THIS PAGE INTENTIONALLY LEFT BLANK

Approved for public release; distribution is unlimited

PERFORMANCE ANALYSIS OF THE EFFECT OF PULSE-NOISE INTERFERENCE ON WLAN SIGNALS TRANSMITTED OVER A NAKAGAMI FADING CHANNEL

Andreas Tsoumanis
Lieutenant Junior Grade, Hellenic Navy
B.S., Hellenic Naval Academy, 1996

Submitted in partial fulfillment of the
requirements for the degree of

MASTER OF SCIENCE IN ELECTRICAL ENGINEERING
and
MASTER OF SCIENCE IN SYSTEMS ENGINEERING

from the

NAVAL POSTGRADUATE SCHOOL
March 2004

Author: Andreas Tsoumanis

Approved by: R. Clark Robertson
Thesis Advisor

Donald Wadsworth
Co-Advisor

Dan C. Boger
Chairman, Department of Information Sciences

John P. Powers
Chairman, Department of Electrical and Computer Engineering

THIS PAGE INTENTIONALLY LEFT BLANK

ABSTRACT

This thesis examines the performance of wireless local area network (WLAN) signals, specifically, the signal of IEEE 802.11a standard. The signal is subject to pulsed-noise jamming, when either the desired signal alone or the desired signal and the jamming signal are subject to Nakagami fading. As expected, the implementation of forward error correction (FEC) coding with soft decision decoding (SDD) and maximum-likelihood detection improves performance as compared to uncoded signals. In addition, the combination of maximum-likelihood detection and error correction coding renders pulsed-noise jamming ineffective as compared to barrage noise jamming. When the jamming signal encounters fading as well, we assume that the average jamming power is much greater than the AWGN power. For uncoded signals, a jamming signal that experiences fading actually improves performance when the parameter of the information signal m_s is less than or equal to one. Surprisingly, for larger values of m_s a jamming signal that experiences fading works in favor of the information signal only for small signal-to-interference ratio (SIR). When SIR is large, performance when the jamming signal experiences fading is worse relative to performance when the jamming signal does not experience fading. For error correction coding with SDD, we investigate only continuous jamming since it is by far the worst-case. Moreover, while we consider a range of fading conditions for the jamming signal, we examine only Rayleigh fading of the information signal. The coded signal, when the jamming signal experiences severe fading, performs better relative to the case when the jamming signal does not experience fading.

THIS PAGE INTENTIONALLY LEFT BLANK

TABLE OF CONTENTS

LIST OF FIGURES

LIST OF TABLES

THIS PAGE INTENTIONALLY LEFT BLANK

ACKNOWLEDGMENTS

This thesis would not have been possible without the initial ideas, the clear explanation and the constant advice of Professor R. Clark Robertson. I gratefully acknowledge his mentorship, and the endless hours he spent answering every question of mine.

I also want to express my sincere appreciation to Professor Donald Wadsworth for his guidance and assistance serving as my co-advisor.

Finally, I want to thank my wife Maria, for her spiritual support and understanding as this work matured.

THIS PAGE INTENTIONALLY LEFT BLANK

EXECUTIVE SUMMARY

The objective of this thesis was to investigate the performance of the effect of pulse-noise jamming on wireless local area network (WLAN) signals transmitted over a Nakagami fading channel. Signal transmission over a mobile channel is subject to fading caused by multipath propagation due to reflections, diffractions, and scattering processes. The Nakagami model of a fading environment is generalized to model different fading conditions. The analysis of both fading and interference are essential to design a robust communications system, especially for military applications, where hostile jamming is expected.

Beginning the analysis when the jamming signal does not encounter fading, we found that the signal without forward error correction (FEC) performs poorly when the signal propagates over a severe fading channel. When FEC with soft decision decoding (SDD) is implemented, the probability of bit error is improved dramatically. This behavior is exhibited for all modulation types and data rates the IEEE 802.11a standard specifies. These results are for a single carrier.

The IEEE 802.11a 5-GHz WLAN standard that we examined implements orthogonal frequency-division multiplexing (OFDM). As will be explained in Chapter II, OFDM can transform a frequency-selective channel to a flat-fading one using orthogonal sub-carriers. The fading effects of a flat-fading channel can be mitigated, and this explains the preference given to OFDM systems when high data rates are required. To continue with the performance analysis for the combined OFDM signal, we assumed independent Nakagami fading for each sub-carrier. Each sub-carrier is assumed to be subject to Nakagami fading with different m, where m is assumed to be uniformly distributed over a specific range. The findings demonstrate the dominance of the negative effects of the more severe conditions, since the overall performance is dominated by the sub-carriers transmitted over channels with small values of m. However, this approach does not examine in depth the distribution of m for the sub-carriers. Thus, it is worst-case and gives only a pessimistic idea of how an OFDM signal performs.

After the evaluation for an unfaded jamming signal, the analysis continues and examines the case for when the jamming signal experiences fading as well. The fading of the interference actually improves the WLAN performance when the desired signal is subject to Rayleigh or more severe fading or when signal-to-interference (SIR) ratio is small, independent of the fading of the desired signal. Surprisingly, for milder fading of the desired signal, fading of the jamming signal increases bit error. When FEC with SDD is implemented the results are similar.

I. INTRODUCTION

A. OBJECTIVE

Wireless local area networks (WLAN) offer increased data rates and reliable performance even when affected by severe fading conditions. These characteristics have made them popular for both commercial and military applications. WLANs are able to operate at high data rates, and their analysis will help achieve an understanding of their limitations and capabilities. The IEEE 802.11a standard is a representative of a WLAN and is adopted for many wireless applications, both military and commercial. This standard supports variable bit rates from six to 54 Mbps and specifies four modulation types: binary phase-shift keying (BPSK), quadrature phase-shift keying (QPSK), 16 quadrature amplitude modulation (16QAM), and 64QAM. Furthermore, it employs forward error correction (FEC) with soft decision decoding (SDD) and orthogonal frequency-division multiplexing (OFDM). OFDM was chosen as a means to overcome the effects of frequency-selective fading conditions.

The scope of this thesis was to investigate the performance of the IEEE 802.11a WLAN waveform transmitted over frequency-selective, slowly fading Nakagami channels. In order to take into account the worst-case scenario, the desired signal is assumed to be subject to pulse-noise jamming. The jamming signal is also assumed to be affected by the fading channel. We make three assumptions for the receiver:

a. the receiver detects the signal coherently,

b. the receiver's local oscillator knows the amplitude of the received signal (maximal-ratio detection), and

c. for FEC with SDD, the receiver maximizes the conditional probability density function of the received code sequence $f_r(r \mid v)$, given the correct code sequence v for equally likely code sequences (maximum-likelihood receiver).

The effect of pulsed-noise jamming was also considered, and the jamming signal was also assumed to encounter fading. Since we assume that the informational signal is

affected by fading, it is reasonable to assume the same for the jamming signal. This thesis attempts to address the cases when the jamming signal is subject to fading or not.

B. RELATED RESEARCH

Numerous works have dealt with the performance of OFDM signals propagating through fading channels. The fading models that have been analyzed vary from Rayleigh and Ricean [1,2] to the more general Nakagami [3]. In [4] Kosa introduced pulsed-noise jamming with FEC and SDD but did not consider SDD for non-binary modulation. This thesis analyzes the performance of IEEE 802.11a receivers with FEC and SDD for both binary and non-binary modulations.

As for the analysis when the jamming signal experiences fading, Oetting in [5] treats the performance of spread spectrum systems when both the envelopes of the desired and the jamming signal fade with a Ricean distribution. References [6] and [7] extended the analysis to accommodate Nakagami fading. All these works focus on frequency-shift keying (FSK) modulations. However, they do not address either the coherent modulation types specified by the IEEE 802.11a standard or FEC with SDD, and this is the focus and novelty of this thesis. Taking into account FEC with SDD, we obtain results that are more generally applicable and will benefit those utilizing a IEEE 802.11a 5-GHz WLAN system.

C. THESIS ORGANIZATION

Apart from the introductory chapter, this thesis comprises four more chapters with the following organization. Chapter II presents the necessary background theory. It includes the Nakagami probability density function and the characteristics of the IEEE 802.11a waveform. The analysis of the next two chapters assumes the information signal is experiencing pulsed-noise jamming and Nakagami, or a special case of Nakagami, fading. Additionally, all modulation types and code rates specified by the standard are examined. In Chapter III we review the performance of an uncoded signal for a single carrier, after the results of [4]. Then the analysis is extended to accommodate FEC with SDD. This chapter concludes with an assumption concerning the effect of fading on the com-

bined OFDM signal, and the resulting performance is discussed. Chapter IV is the bulk of this thesis. Its structure is similar to Chapter III, with the difference that the jamming signal is assumed to experience fading as the information signal does. The analysis begins by investigating the performance of an uncoded signal for a single carrier and continues with the study of FEC with SDD. Chapter V summarizes all findings and comments the most important results. Finally, we conclude with recommendations for further research.

THIS PAGE INTENTIONALLY LEFT BLANK

II. THEORY REVIEW

A. INTRODUCTION

Before proceeding to the analysis, it is prudent to review some background. Initially, we present the characteristics of the Nakagami fading channel. We present the Nakagami density function and explain the reason it is selected to model the fading channel. Then, we look at the characteristics of the IEEE 802.11a signal. Specifically, we state the different modulation types the standard specifies and the corresponding data rates, as well as discussing briefly convolutional coding and OFDM.

B. NAKAGAMI FADING MODEL

The distribution we selected to model the fading channel is the Nakagami distribution. The reason is its flexibility and accuracy in matching experimental data. Changing the m parameter of the distribution, we can model a wide variety of fading conditions. The Rayleigh fading channel is a special case with $m = 1$, one-sided Gaussian fading is a special case with $m = 1/2$, and non-fading is a special case that occurs when m approaches infinity.

The Nakagami-m density function is a function of two parameters, r and Ω, and is given by [8] as:

$$f_R(r) = \frac{2}{\Gamma(m)}\left(\frac{m}{\Omega}\right)^m r^{2m-1} e^{-\frac{mr^2}{\Omega}}, \tag{2.1}$$

where Ω is defined as

$$\Omega = E[R^2]. \tag{2.2}$$

$\Gamma(m)$ is the Gamma function defined as

$$\Gamma(m) = \int_0^\infty t^{m-1} e^{-t} dt, \qquad m \geq 0 \tag{2.3}$$

and the m parameter is expressed as

$$m = \frac{\Omega^2}{E[(R^2 - \Omega)^2]}, \qquad m \geq \frac{1}{2}. \tag{2.4}$$

In Figure 1 we see the probability density function of the Nakagami distribution for different values of m.

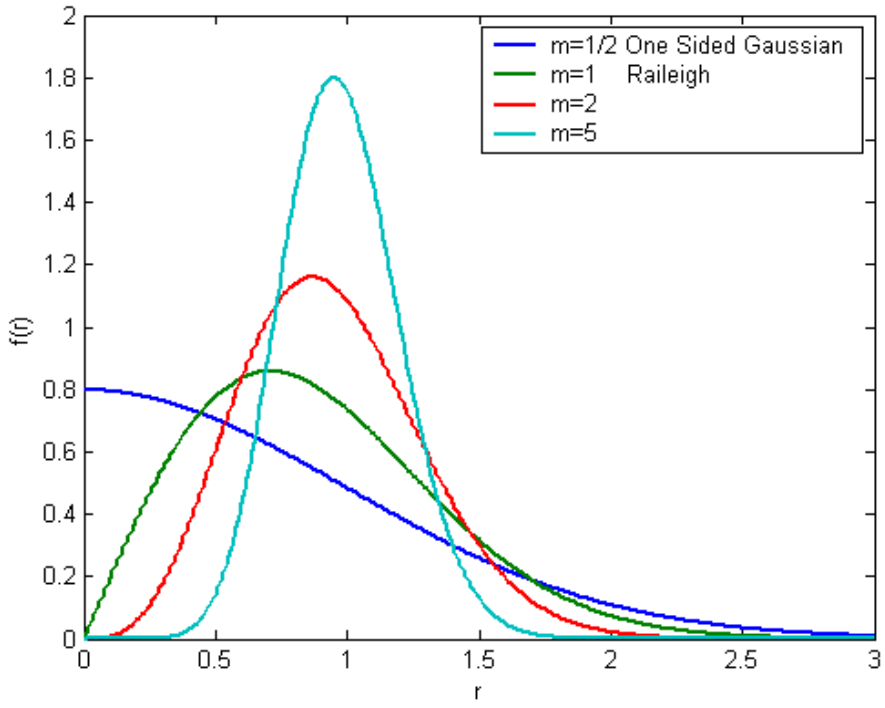

Figure 1. The Nakagami probability density function [After Ref. 8.].

C. WAVEFORM CHARACTERISTICS

1. Single Carrier Modulation Types

The modulation types implemented by IEEE 802.11a standard for a single carrier are BPSK, QPSK, 16QAM, or 64QAM. These four types were selected for two properties they have in common. First, they are bandwidth efficient, a critical feature for a WLAN system, where increased data rates are required. Second, they can be easily implemented, reducing the cost of hardware. By definition the signals of MPSK and MQAM are very similar. We know that for a rectangular signal constellation the power spectral density, transmission bandwidth, and spectral efficiency of MQAM are identical to those of MPSK [9]. The constellations for 16QAM and 64QAM specified by the IEEE

802.11a standard are square and are shown in Figure 2 [10]. Like MPSK, MQAM utilizes both the in-phase and the quadrature component of the carrier. Both MPSK and MQAM

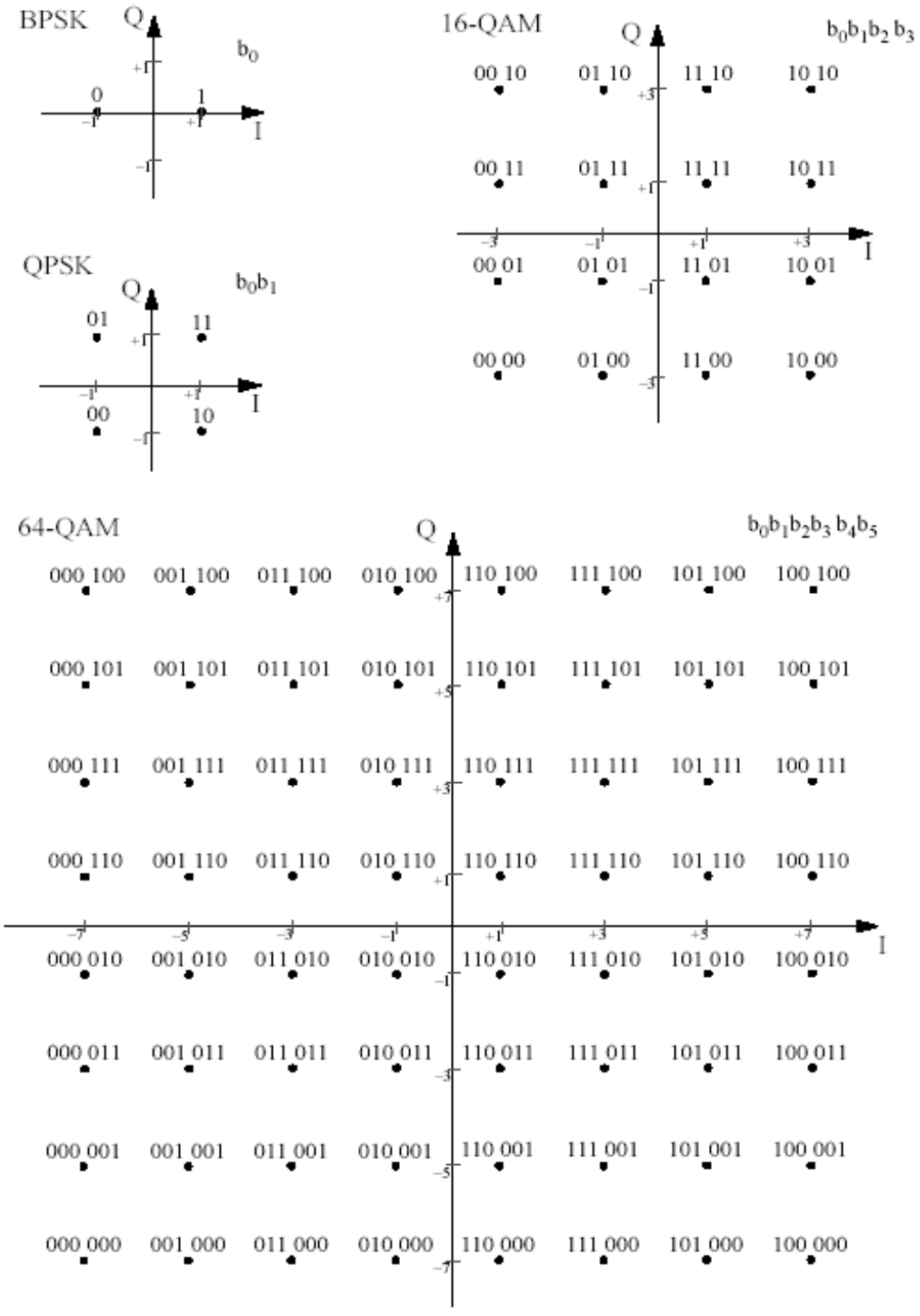

Figure 2. Constellation for BPSK, QPSK, 16QAM, and 64QAM [From Ref. 10.].

demodulate the two components of the carrier independently and can be thought of as two independent M-ary pulse amplitude modulation (MPAM) signals. Due to this, it is easy to implement a receiver for each of these modulation types using the same hardware. In Chapters III and IV, we investigate the performance obtained with each of the modulation types.

2. Forward Error Correction (FEC)

In order to overcome performance degradation due to multipath fading, the IEEE 802.11a standard employs FEC. With FEC, redundant bits are added to the raw data stream. The IEEE 802.11a standard specifies the convolutional encoder of Figure 3, which uses six linear shift-register stages [10]. In general a convolutional code takes k input bits and generates n coded output bits. The ratio $r = k/n$ is defined as the code rate and is indicative of the number of redundant bits in the bit stream. The code rates specified by the standard depend on the modulation type and the desired data rate. Table 1 gives the modulation type each code rate is combined with and the achieved data rate.

Table 1. Rate-dependent parameters [From Ref. 10.].

Data rate (Mbps)	Modulation	Code Rate
6	BPSK	1/2
9	BPSK	3/4
12	QPSK	1/2
18	QPSK	3/4
24	16QAM	1/2
36	16QAM	3/4
48	64QAM	2/3
54	64QAM	3/4

Another parameter that specifies the convolutional code is the constraint length ν. According to [11], ν is the maximum number of coded bits that can be affected by a single information bit. The convolutional encoder employed by IEEE 802.11a for

$r = 1/2$ has a constraint length $\nu = 7$ and is shown in Figure 3. The less redundant code rates of 2/3, and 3/4 are derived from it through puncturing. Puncturing implies that some of the encoded bits are omitted so that the number of the transmitted bits is reduced, and the code rate is increased. The omitted bits are replaced by dummy "zero" bits. These dummy bits are accounted for by the decoder.

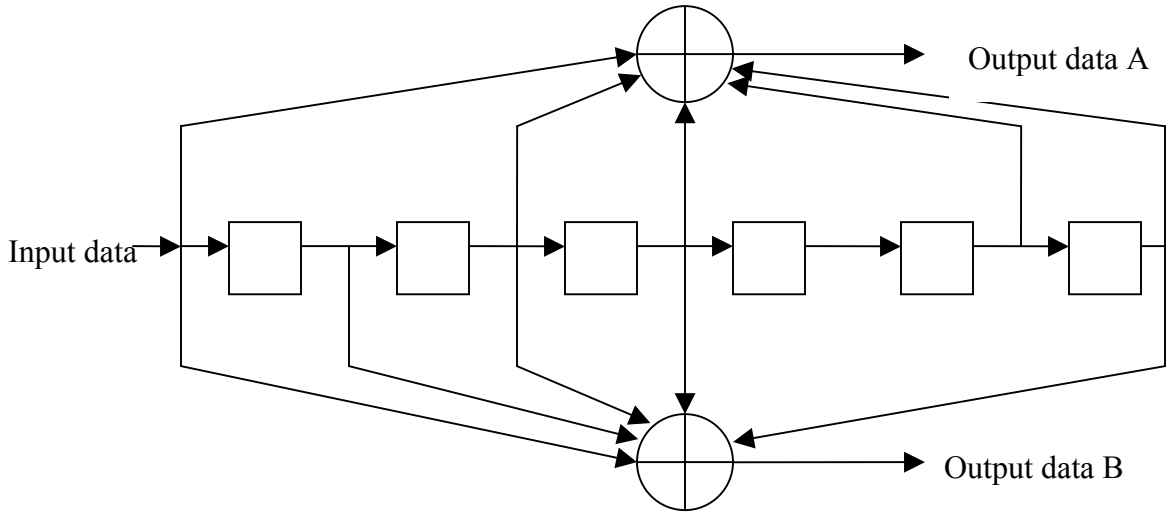

Figure 3. Convolutional encoder with $\nu = 7$ and $r = 1/2$, where the empty boxes denote shift registers [After Ref. 10.].

3. Orthogonal Frequency-Division Multiplexing (OFDM)

OFDM is a signaling technique that transmits the data bits on a number of orthogonal carrier frequencies or sub-carriers. If the number of available sub-carrier frequencies are *N*, the data rate for an individual sub-carrier is $R_{b_c} = R_b / N$, where R_b is the overall data rate [12]. Thus, the required bandwidth for each sub-carrier is reduced by a factor of *N*. The orthogonality of the carrier frequencies is another feature of OFDM that minimizes the overall signal bandwidth. The bandwidth of the individual sub-carrier signals overlaps each other, yielding an overall bandwidth savings. The IEEE 802.11a standard specifies 52 sub-carriers, 48 of which are used for transmitting information bits and the rest for transmitting pilot tones.

Besides reduced signal bandwidth, OFDM is effective when the signal is transmitted over a fading channel. If the IEEE 802.11a standard specified only one carrier, the

high data rate would cause the noise equivalent bandwidth (W) of the signal to exceed the coherence bandwidth of the channel $(\Delta f)_c$ [9]. In this case $W > (\Delta f)_c$, and the channel is said to be frequency-selective. As a result, the distortion of the signal is significant. For each sub-carrier of an OFDM signal, the noise equivalent bandwidth W_c is reduced by N and is less than the coherence bandwidth of the channel $W_c = W/N < (\Delta f)_c$. Hence, the channel is characterized as flat-fading for each individual sub-carrier.

While the use of N sub-carriers reduces the bandwidth, it increases bit duration or symbol duration, depending on the modulation type, as:

$$T_{b_c} = NT_b . \tag{2.5}$$

If we let N get very large, the bit duration of each carrier may become larger than channel coherence time $T_{b_c} > (\Delta t)_c$, and the channel is then characterized as fast fading. In a fast fading channel, the channel impulse response changes rapidly within the bit duration. This causes frequency dispersion due to Doppler spreading, which leads to signal distortion [13]. To avoid the latter, the channel must remain slowly fading and that limits the maximum allowable value of N.

Figure 4 illustrates the generation of an OFDM signal, where we see the transmitter and receiver block diagram. On the transmitter side, the information bits are first convolutionally encoded by the encoder of Figure 3. Then, a block interleaver, defined by a two-step permutation, interleaves the coded bits. The first permutation ensures that adjacent coded bits are mapped onto nonadjacent sub-carriers. The second ensures that adjacent coded bits are mapped alternatively onto less and more significant bits of the constellation of Figure 2 [10]. Spreading the bits over time prevents the important bits of a block of source bits from being corrupted when there is a deep fade or noise burst.

After the interleaver stage, data are mapped. They are divided into groups of one, two, four, or six bits and converted into complex numbers representing BPSK, QPSK, 16QAM, or 64QAM constellation points, respectively. The inverse fast Fourier transform (IFFT) transforms these symbols into a complex baseband signal. The smoothness of the

transition from symbol to symbol is done by windowing, narrowing the output spectrum. Next, the OFDM symbol modulates the two orthogonal carriers, is upconverted, amplified and transmitted.

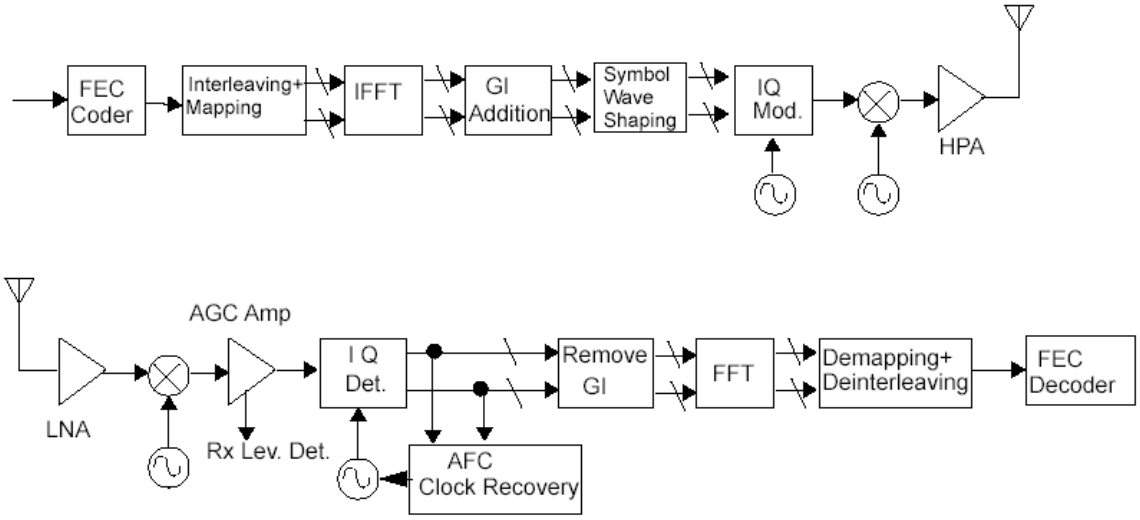

Figure 4. Transmitter and receiver block diagram for the OFDM PHY [After Ref. 10.].

D. SUMMARY

In this chapter, we addressed Nakagami-*m* distribution and explained the reasons we selected it to model the fading channel. Then, we stated the characteristics of the IEEE 802.11a standard signal: modulation types of a single sub-carrier, error correction coding, and orthogonal frequency-division multiplexing. In the next chapter, we will investigate in detail the effect of fading and pulsed-noise jamming on a WLAN signal.

THIS PAGE INTENTIONALLY LEFT BLANK

III. PERFORMANCE ANALYSIS WITH FEC AND SDD FOR SIGNALS TRANSMITTED OVER A NAKAGAMI FADING CHANNEL WITH PULSED-NOISE JAMMING

A. INTRODUCTION

In the previous chapter, we examined all the necessary background required to understand the basic principles of the IEEE 802.11a wireless local area network standard. Now it is time to see how these principles are applied in practice by proceeding to the performance analysis. We examined the different modulation types separately for the coded and uncoded case. In [3] and [4], whose work was continued in this thesis, the analysis included the performance of coded signals, decoded with both hard decision decoding (HDD) and soft decision decoding (SDD). Since this thesis was concentrated solely on the actual characteristics of the IEEE 802.11a wireless local area network standard, in addition to no coding, we examined only SDD. Especially for M-ary QAM, we addressed specific assumptions made to analyze non-binary signals with SDD.

Lastly, we expanded our results to the combined OFDM signal and examined the effect of fading when all 48 sub-carriers are considered one signal. In all cases we assumed the signal experienced frequency-selective, slow Nakagami fading and pulsed-noise jamming.

B. BPSK/QPSK

These two modulation types were examined together since they are both analyzed in the same way. A QPSK signal is a special case of M-ary PSK that enjoys double the data rate of BPSK, since both the in-phase and the quadrature component of the carrier are utilized.

1. Without SDD

The material of this section has been derived in [4] and the probability of bit error rate is restated here:

$$P_{b_{BPSK/QPSK}} = \frac{p}{\sqrt{1+m\left(\mathrm{SNR}^{-1}+\mathrm{SIR}^{-1}/p\right)}} \frac{\Gamma(m+0.5)}{2\sqrt{\pi}\Gamma(m+1)\left(1+\dfrac{1}{m\left(\mathrm{SNR}^{-1}+\mathrm{SIR}^{-1}/p\right)}\right)^{m}}$$

$$\times\left(1+\sum_{k=0}^{\infty}\left(\prod_{i=1}^{k}\frac{m+i-0.5}{m+i}\left(\frac{1}{1+\left(m(\mathrm{SNR}^{-1}+\mathrm{SIR}^{-1}/p)\right)^{-1}}\right)^{k}\right)\right)$$

$$+\frac{1-p}{\sqrt{1+\dfrac{m}{\mathrm{SNR}}}} \frac{\Gamma(m+0.5)}{2\sqrt{\pi}\Gamma(m+1)\left(1+\dfrac{\mathrm{SNR}}{m}\right)^{m}}\left(1+\sum_{k=0}^{\infty}\left(\prod_{i=1}^{k}\frac{m+i-0.5}{m+i}\left(\frac{1}{1+\dfrac{\mathrm{SNR}}{m}}\right)^{k}\right)\right). \quad (3.1)$$

In Figure 5 we can see the performance of BPSK/QPSK for different values of m. The obvious characteristic concerning the effect of m is that, as it increases, we approach the non-fading case. For small values of m, fading is severe and there is considerable performance reduction.

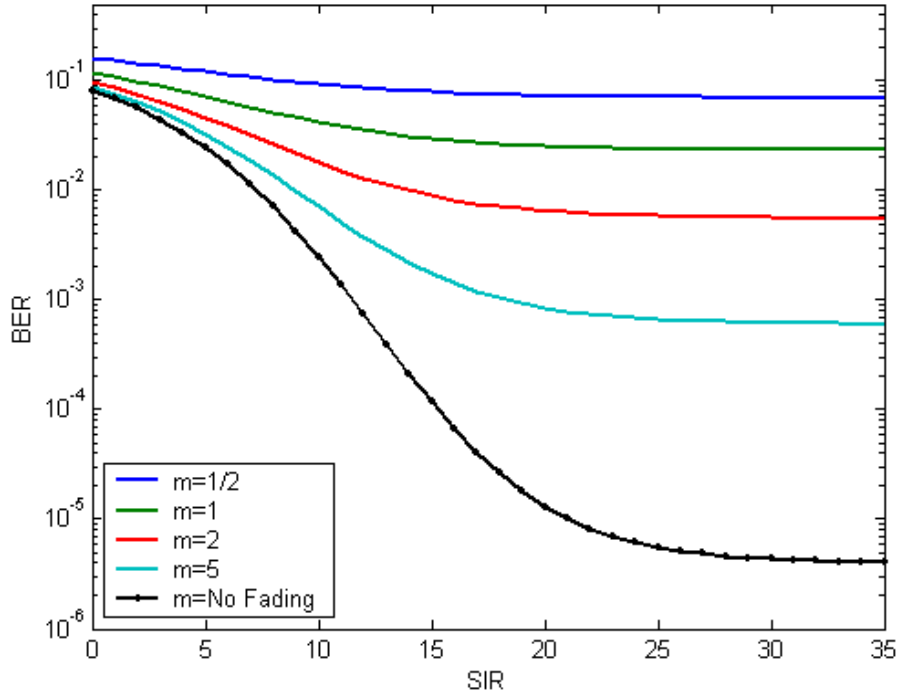

Figure 5. BPSK/QPSK for $\mathrm{SNR} = 10\,\mathrm{dB}$ and $p = 0.5$ [After Ref. 4.].

In Figure 6 we plot the probability of bit error for the Rayleigh fading channel ($m = 1$) using different values of p, the fraction of time the jammer is on. We note the jammer is more effective when the jamming is continuous. This is obvious for small SIR, while for larger SIR the value of p does not play any role.

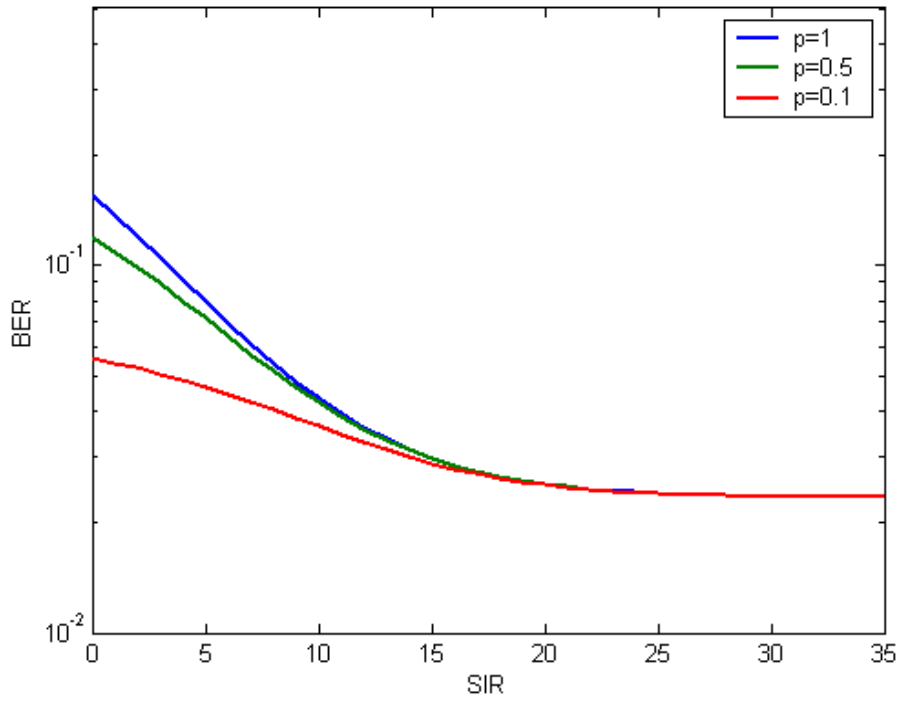

Figure 6. BPSK/QPSK for SNR = 10 dB, and $m = 1$ [After Ref. 4.].

In Figure 7 the m parameter is larger ($m = 5$), indicating much better fading conditions than Rayleigh (usually specifying a line-of-sight (LOS) between the workstation and the access point). The results are very different compared to those obtained for Rayleigh fading. For mid-range values of SIR, the effectiveness of the jammer is improved for small p. This is consistent with the results obtained when there is no fading. In all three figures, when m is small the bit error rate is too large, and this explains why convolutional coding is used in the IEEE 802.11a standard, which is discussed in the next section.

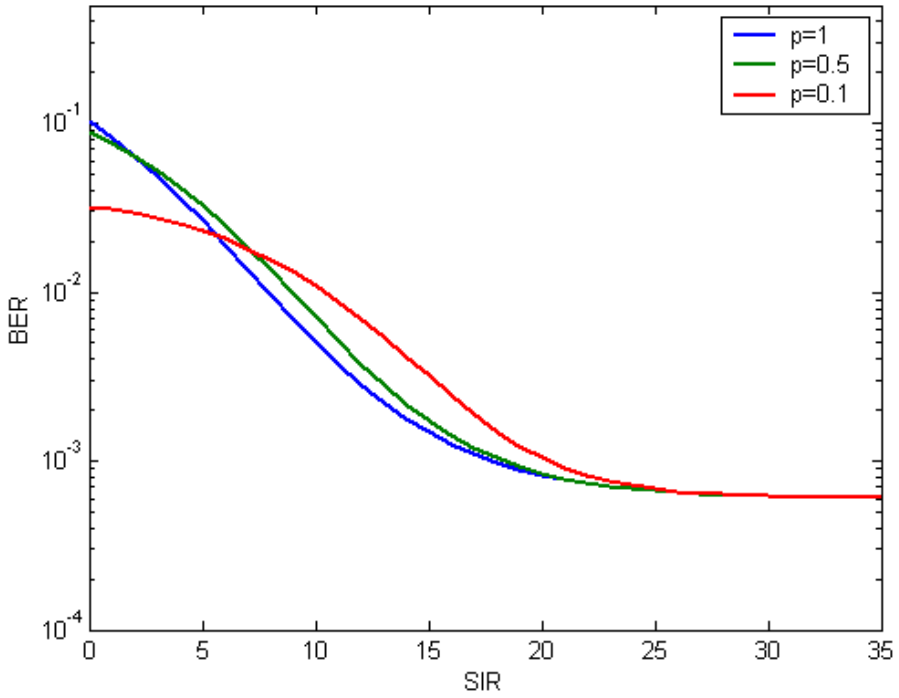

Figure 7. BPSK/QPSK for SNR = 10 dB, $m = 5$, and $p = 0.5$ [After Ref. 4.].

2. With FEC and SDD

In [14], Proakis gives the widely accepted upper bound on the probability of bit error (P_b), since the exact solution cannot be derived, as

$$P_b < \frac{1}{k} \sum_{d=d_{free}}^{\infty} B_d P_d \,. \tag{3.2}$$

In the above inequality, k is the number of information bits encoded per clock cycle and the numerator of the code rate r, d is the weight of the path, d_{free} represents the minimum Hamming distance between all pairs of complete convolutional code sequences, B_d is the sum of all possible bit errors that can occur when a path of weight d is selected, and P_d represents the probability that the decoder will select a path of weight d.

The values of B_d cannot in general be computed, but have been determined by extensive computer search for optimal performance for a constraint length ν and code

rate r convolutional code. After [10], in Table 2 the values of B_d are shown for the codes specified by the IEEE 802.11a standard.

Table 2. Weight Structure of the Best Convolutional Codes [After Ref. 10.].

Code Rate	d_{free}	$B_{d_{free}}$	$B_{d_{free}+1}$	$B_{d_{free}+2}$	$B_{d_{free}+3}$	$B_{d_{free}+4}$
1/2	10	36	0	211	0	1404
2/3	6	1	81	402	1487	6793
3/4	5	21	252	1903	11995	72115

According to [12], the sum in Inequality (3.2) is dominated by the first five non-zero terms of the summation.

From this point on, the analysis diverges depending on whether we are dealing with SDD or HDD. To continue with SDD, we expand the approach of [4] in order to accommodate the case when the receiver has no information whether a bit is jammed or not. Consequently, we have to find P_d so as to be able to evaluate Inequality (3.2). For optimum performance the use of a maximum-likelihood receiver is required. A maximum-likelihood receiver maximizes the conditional probability density function of the received code sequence $f_r(r \mid v)$ given the correct code sequence v for equally likely code sequences. For the BPSK/QPSK signal, the output of the demodulator for each bit r_l is modeled as a Gaussian random variable with mean $\overline{r} = \sqrt{2}a_{c_l}$ and variance σ_l^2. If the correct path is the all-zero path and the r^{th} path differs from the correct path in d bits, then a decoding error occurs when [14]

$$\sum_{l=1}^{d} \frac{a_{c_l} r_l}{\sigma_l^2} > 0 . \tag{3.3}$$

In the preceding equation the index l runs over the set of d bits in which the r^{th} path differs from the correct path, r_l is the demodulator output, a_{c_l} is the amplitude of

the received signal and is modeled as a random variable due to the effect of the fading channel, and σ_l^2 is the power of the noise for each bit, which we must know in order to distinguish between bits that are jammed and those that are not. The probability P_d is simply

$$P_d = P_r\left(\sum_{l=1}^{d} \frac{a_{c_l} r_l}{\sigma_l^2} > 0\right). \tag{3.4}$$

We define

$$z_l = \frac{a_{c_l} r_l}{\sigma_l^2}. \tag{3.5}$$

Obviously, after this transformation of random variables z_l remains a Gaussian random variable with mean $\bar{z}_l = \sqrt{2} a_{c_l}^2 / \sigma_l^2$ and variance $a_{c_l}^2 / \sigma_l^2$. We now introduce z as the sum of d independent random variables

$$z = \sum_{l=1}^{d} z_l, \tag{3.6}$$

where z is a Gaussian random variable since it is the summation of independent Gaussian random variables. The mean of z is $\bar{z} = \sqrt{2} \sum_{l=1}^{d} a_{c_l}^2 / \sigma_l^2$ and the variance is $\sum_{l=1}^{d} a_{c_l}^2 / \sigma_l^2$.

Combining Equations (3.4) and (3.6), we get

$$P_d = P_r(z > 0). \tag{3.7}$$

Expressing P_d in terms of the Q-function, we can write

$$P_d = Q\left(\sqrt{\frac{\bar{z}^2}{\sigma_z^2}}\right) = Q\left(\sqrt{\frac{2\left(\sum_{l=1}^{d} \frac{a_{c_l}^2}{\sigma_l^2}\right)^2}{\sum_{l=1}^{d} \frac{a_{c_l}^2}{\sigma_l^2}}}\right) = Q\left(\sqrt{2\left(\sum_{l=1}^{d} \frac{a_{c_l}^2}{\sigma_l^2}\right)}\right). \tag{3.8}$$

In order to take into account pulsed-noise jamming, we split the sum of $a_{c_l}^2 / \sigma_l^2$ over the d bits:

$$P_d = Q\left(\sqrt{2\left(\frac{\sum_{l=1}^{i} a_{c_l}^2}{\sigma_t^2} + \frac{\sum_{l=i+1}^{d} a_{c_l}^2}{\sigma_o^2}\right)}\right). \tag{3.9}$$

The first part of the sum in the argument of the Q-function corresponds to i jammed bits, while σ_t^2 represents the total noise power (AWGN plus jamming noise). The latter part of the sum corresponds to $d-i$ unjammed bits where only the AWGN noise power σ_o^2 is present.

If we express

$$h = \frac{\sum_{l=1}^{i} a_{c_l}^2}{\sigma_t^2} + \frac{\sum_{l=i+1}^{d} a_{c_l}^2}{\sigma_o^2}, \tag{3.10}$$

then we see that P_d is conditional on h. To obtain the unconditional P_d, we integrate $P_d(h)$ multiplied by the probability density function of h ($f_H(h)$) over the values for which h is valid:

$$P_d = \int_0^{\infty} P_d(h) f_H(h)\, dh. \tag{3.11}$$

In order to proceed, we must find $f_H(h)$. We know the Nakagami-m probability density function is given by

$$f_{Ac}(a_c) = \frac{2}{\Gamma(m)}\left(\frac{m}{\overline{a_c^2}}\right)^m a_c^{2m-1} e^{-\frac{m a_c^2}{\overline{a_c^2}}}. \tag{3.12}$$

First, we expand Equation (3.12) in order to compute the probability density function of a squared random variable. Next, we must obtain the pdf of the sum of i independent squared random variables, which is given by [3] as

$$f_{B1}(b1) = \frac{1}{\Gamma(mi)}\left(\frac{m}{\overline{b}}\right)^{mi} b1^{mi-1} e^{-\frac{m\,b1}{\overline{b}}} \tag{3.13}$$

where the random variable $b1$ is defined as

$$b1 = \sum_{l=1}^{i} a_{c_l}^2 , \tag{3.14}$$

and $\overline{b}$ is the average power of the signal. Analogously, the pdf of the sum of $d-i$ independent squared random variables is

$$f_{B2}(b2) = \frac{1}{\Gamma\big(m(d-i)\big)}\left(\frac{m}{\overline{b}}\right)^{m(d-i)} b2^{m(d-i)-1} e^{-\frac{m\,b2}{\overline{b}}} , \tag{3.15}$$

where

$$b2 = \sum_{l=i+1}^{d} a_{c_l}^2 . \tag{3.16}$$

Substituting Equations (3.14) and (3.16) into Equation (3.10), we get

$$h = \frac{b1}{\sigma_t^2} + \frac{b2}{\sigma_o^2} = h1 + h2 . \tag{3.17}$$

Next, we must find the pdfs of $h1$ and $h2$. From Equation (3.17),

$$h1 = \frac{b1}{\sigma_t^2}, \qquad \frac{db1}{dh1} = \sigma_t^2 . \tag{3.18}$$

We know that

$$f_{H1}(h1) = \frac{|\,db1\,|}{|\,dh1\,|} f_{B1}(b1)\,|_{b1=f^{-1}(h1)} \tag{3.19}$$

Substituting Equations (3.13) and (3.18) into Equation (3.19), we get

$$f_{H1}(h1) = \frac{1}{\Gamma(mi)}\left(\frac{m}{\overline{b}}\right)^{mi} (\sigma_t^2)^{mi}\, h1^{mi-1} e^{-\frac{m\,\sigma_t^2\,h1}{\overline{b}}} . \tag{3.20}$$

Following the same methodology, we obtain the pdf of $h2$ as

$$f_{H2}(h2) = \frac{1}{\Gamma\big(m(d-i)\big)}\left(\frac{m}{\overline{b}}\right)^{m(d-i)} (\sigma_o^2)^{m(d-i)} h2^{m(d-i)-1} e^{-\frac{m\sigma_o^2 h2}{\overline{b}}}. \tag{3.21}$$

The last step is to find the pdf of the sum of $h1+h2$. It is given by the convolution of the two separate pdfs. However, we will take advantage of the relevant property of the Laplace transformation, stating that convolution is equivalent to multiplication in the Laplace domain. Thus, we multiply the two pdfs after their transformation into the Laplace domain. Since the pdf is non-zero only for positive arguments,

$$\mathcal{L}\{f_{H1}(h1)\} = F_{H1}(s) = \int_0^\infty f_{H1}(h1) e^{-sh1} dh1 \tag{3.22}$$

where $\mathcal{L}\{\bullet\}$ indicates the Laplace transform operator. Substituting Equation (3.20) into (3.22), we get

$$F_{H1}(s) = \int_0^\infty \frac{1}{\Gamma(mi)}\left(\frac{m}{\overline{b}}\right)^{mi} (\sigma_t^2)^{mi} h1^{mi-1} e^{-\frac{m\sigma_t^2 h1}{\overline{b}}} e^{-sh1} dh1 \tag{3.23}$$

which can be simplified to

$$F_{H1}(s) = \left(\frac{m}{\overline{b}}\right)^{mi} (\sigma_t^2)^{mi} \frac{1}{\Gamma(mi)} \int_0^\infty h1^{mi-1} e^{-\left(s+\frac{m\sigma_t^2}{\overline{b}}\right)h1} dh1. \tag{3.24}$$

Using the Laplace transform pair

$$\mathcal{L}\left\{\frac{t^{u-1}}{\Gamma(u)} e^{-at}\right\} = \frac{1}{(s+a)^u} \qquad \text{for } u > 0, \tag{3.25}$$

we set

$$t = h1_c, \tag{3.26}$$

$$u = mi, \tag{3.27}$$

and

$$a = s + \frac{m\sigma_t^2}{\overline{b_c}}, \tag{3.28}$$

which allows us to get

$$F_{H1}(s) = \left(\frac{m}{\overline{b}}\right)^{mi} (\sigma_t^2)^{mi} \frac{1}{\left(s + \frac{m\sigma_t^2}{\overline{b}}\right)^{mi}}. \tag{3.29}$$

Similarly,

$$\mathcal{L}\{f_{H2}(h2)\} = F_{H2}(s) = \int_0^\infty f_{H2}(h2) e^{-sh2} dh2 \tag{3.30}$$

which can be evaluated to yield

$$F_{H2}(s) = \left(\frac{m}{\overline{b}}\right)^{m(d-i)} (\sigma_o^2)^{m(d-i)} \frac{1}{\left(s + \frac{m\sigma_o^2}{\overline{b}}\right)^{m(d-i)}}. \tag{3.31}$$

The pdf of h in the Laplace domain is the product of $\mathcal{L}\{f_{H1}(h1)\}$ and $\mathcal{L}\{f_{H2}(h2)\}$:

$$\mathcal{L}\{f_H(h)\} = F_H(s) = \mathcal{L}\{f_{H1}(h1)\}\mathcal{L}\{f_{H2}(h2)\}. \tag{3.32}$$

Hence, substituting Equations (3.29) and (3.31) into Equation (3.32), we get

$$F_H(s) = \left(\frac{m}{\overline{b}}\right)^{mi} (\sigma_t^2)^{mi} \frac{1}{\left(s + \frac{m\sigma_t^2}{\overline{b}}\right)^{mi}} \left(\frac{m}{\overline{b}}\right)^{m(d-i)} (\sigma_o^2)^{m(d-i)} \frac{1}{\left(s + \frac{m\sigma_o^2}{\overline{b}}\right)^{m(d-i)}} \tag{3.33}$$

which can be simplified to

$$F_H(s) = \left(\frac{m}{\overline{b}}\right)^{md} \frac{(\sigma_t^2)^{mi}(\sigma_o^2)^{m(d-i)}}{\left(s + \frac{m\sigma_t^2}{\overline{b}}\right)^{mi}\left(s + \frac{m\sigma_o^2}{\overline{b}}\right)^{m(d-i)}}. \tag{3.34}$$

To write Equation (3.34) in terms of SNR and SIR we define

$$\text{SNR} = \frac{\overline{b}}{\sigma_o^2} \tag{3.35}$$

and

$$\text{SIR} = \frac{\overline{b}}{\sigma_j^2}, \tag{3.36}$$

where σ_o^2 is the power of the AWGN and σ_j^2 is the noise power of the jamming signal. Combining both powers, we get the total power

$$\sigma_t^2 = \sigma_o^2 + \sigma_j^2 . \tag{3.37}$$

The resulting signal-to-noise plus interference ratio is

$$\text{SNIR} = \frac{\bar{b}}{\sigma_t^2} = \frac{\bar{b}}{\sigma_o^2 + \sigma_j^2} = \frac{1}{\frac{\sigma_o^2}{\bar{b}} + \frac{\sigma_j^2}{\bar{b}}} \tag{3.38}$$

which can be written

$$\text{SNIR} = \frac{1}{\text{SNR}^{-1} + \text{SIR}^{-1}} = \left(\text{SNR}^{-1} + \text{SIR}^{-1}\right)^{-1}. \tag{3.39}$$

Now we can rewrite Equation (3.34) as

$$F_{H_c}(s) = \frac{\left(\text{SNR}^{-1} + \text{SIR}^{-1}\right)^{mi} \text{SNR}^{-m(d-i)} m^{md}}{\left(s + \frac{m}{\left(\text{SNR}^{-1} + \text{SIR}^{-1}\right)^{-1}}\right)^{mi} \left(s + \frac{m}{\text{SNR}}\right)^{m(d-i)}} . \tag{3.40}$$

The inverse Laplace transform of the equation above is too complicated to calculate directly. Alternatively, we use the methodology [9] of the numerical inverse of the two-sided Laplace transform. The latter is defined as

$$\mathcal{L}\{f_X(x)\} = F_X(s) = \int_{-\infty}^{\infty} f_X(x) e^{-sx} dx . \tag{3.41}$$

The inverse two-sided Laplace transform is given by

$$\mathcal{L}^{-1}\{F_X(s)\} = f_X(x) = \frac{1}{2\pi j} \int_{c-j\infty}^{c+j\infty} F_X(s) e^{sx} ds . \tag{3.42}$$

where c must be within the strip of convergence of $F_X(s)$ [9]. By successive changes of variables we get

$$f_X(x) = \frac{ce^{cx}}{\pi} \int_0^{\pi/2} \Big[\mathrm{Re}\{F_X(c + jc\tan\phi)\} \cos(cx\tan\phi)$$

$$- \mathrm{Im}\{F_X(c + jc\tan\phi)\} \sin(cx\tan\phi) \Big] \sec^2\phi \; d\phi \,. \qquad (3.43)$$

Rewriting Equation (3.43) in terms of the notation used, we have

$$f_H(h) = \frac{ce^{cx}}{\pi} \int_0^{\pi/2} \Big[\mathrm{Re}\{F_H(c + jc\tan\phi)\} \cos(cx\tan\phi)$$

$$- \mathrm{Im}\{F_H(c + jc\tan\phi)\} \sin(cx\tan\phi) \Big] \sec^2\phi \; d\phi \,. \qquad (3.44)$$

Up to this point we have evaluated $P_d(i)$. Next, we find P_d independent of i. The probability of selecting a path that is a Hamming distance d from the correct path when i of the d bits are jammed for BPSK/QPSK is the sum of the probability that one bit is jammed and $d-1$ are not, plus the probability of two bits are jammed and $d-2$ are not, etc., and is expressed as

$$P_d = \sum_{i=0}^{d} P_r(i \text{ bits jammed}) P_d(i) \,, \qquad (3.45)$$

where $P_d(i)$ is found by substituting Equation (3.44) in Equation (3.11). The probability $P_r(i \text{ bits jammed})$ is

$$P_r(i \text{ bits jammed}) = \binom{d}{i} p^i (1-p)^{d-i} \,. \qquad (3.46)$$

where p is the fraction of time the jammer is on. Now Equation (3.45) is written as

$$P_d = \sum_{i=0}^{d} \binom{d}{i} p^i (1-p)^{d-i} P_d(i) \,. \qquad (3.47)$$

We have almost concluded the analysis, but we must take into account two more things. The first is the assumption that the average jamming power remains constant, independent of p. This statement implies that instantaneous jamming power increases when the jammer is on. Thus, SIR is replaced with

$$\mathrm{SIR}' = \frac{\mathrm{SIR}}{p}. \tag{3.48}$$

The second thing is the relation between the average energy of the uncoded data bit E_b and the coded one E_{b_c}. The uncoded data rate R_b is r times the coded data rate R_{b_c},

$$R_b = r R_{b_c}. \tag{3.49}$$

In addition, the average transmitted power is the same whether coded or uncoded bits are transmitted. Hence,

$$P = E_{b_c} R_{b_c} = E_b R_b \tag{3.50}$$

and

$$E_{b_c} = \frac{R_b}{R_{b_c}} E_b = r E_b. \tag{3.51}$$

This means that the power of coded bits is r times the power of uncoded bits. To compensate for this, we must multiply the expressions for uncoded bit power (SNR and SIR) by the code rate r.

In light of Equation (3.47) and the considerations of the previous two paragraphs, we can now numerically evaluate Equation (3.11). With the values in Table 2 for B_d, we can then calculate Equation (3.2). For the code rate $r = 1/2$, which is used for data rates of six Mbps (BPSK) and 12 Mbps (QPSK), we get Figures 8 and 9 for different values of SNR (10 dB and 16 dB, respectively). The points of interest in the Figures are, firstly, the fact that as SIR increases the probability of error converges to the value corresponding to no jamming. Second, it is obvious that the jamming signal is far more efficient when employing continuous jamming ($p = 1$).

Taking as a reference the performance for $P_b = 10^{-4}$, the comparison between the curves for $p = 1$ and $p = 0.5$ yields a difference of seven dB for $\mathrm{SNR} = 10\,\mathrm{dB}$. What is more, the performance for $p = 0.1$ is small even for small values of SIR. Undoubtedly, maximum-likelihood detection with SDD deprives the jammer of using pulsed-noise techniques. Pulsed-noise jamming techniques are preferred when attacking a communi-

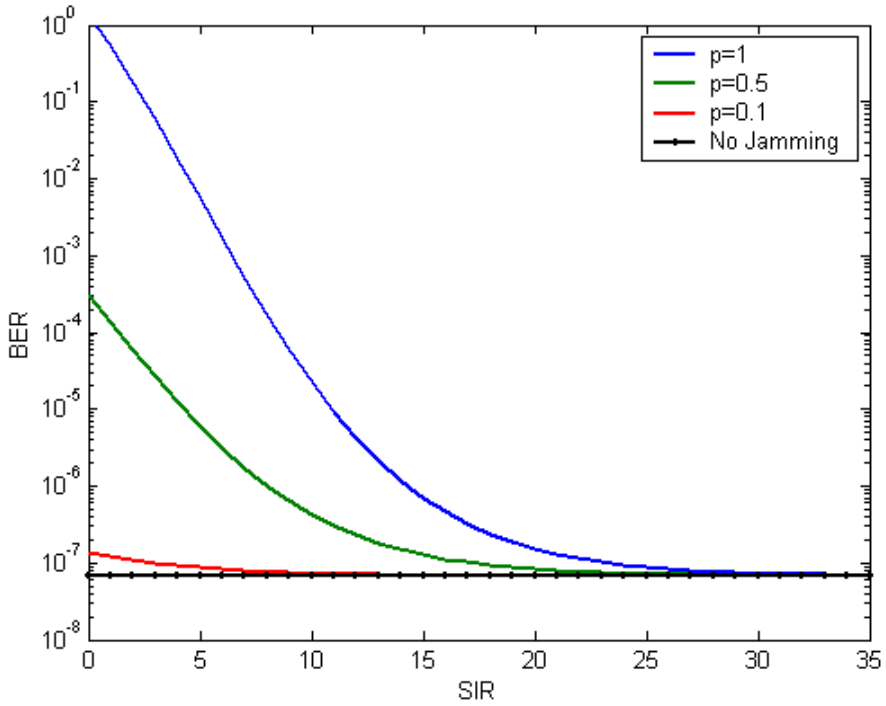

Figure 8. BPSK/QPSK ($r = 1/2$) with FEC and SDD for signals transmitted over a Nakagami fading channel ($m = 1$) with pulsed-noise jamming (SNR $= 10$ dB).

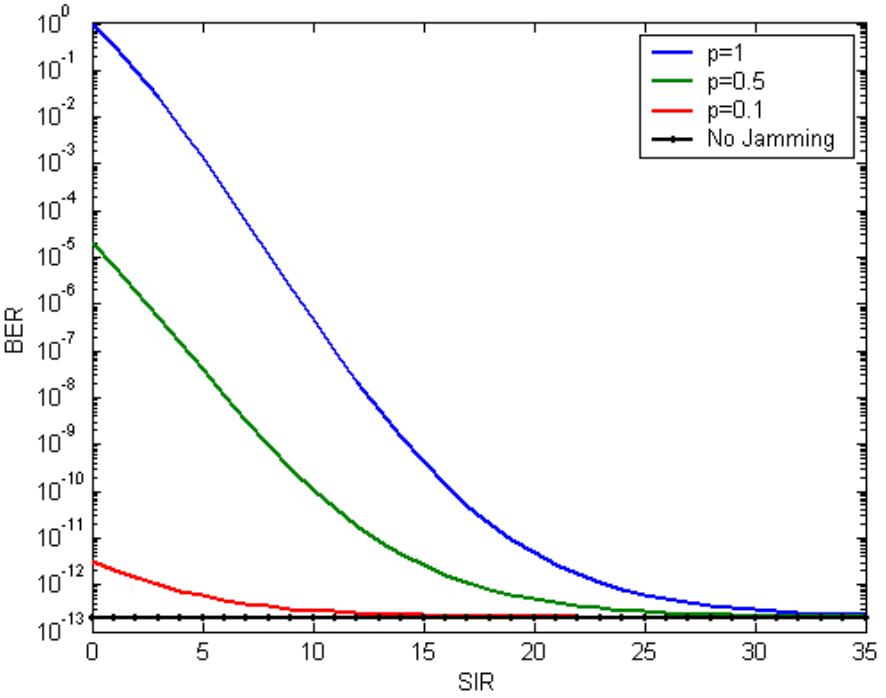

Figure 9. BPSK/QPSK ($r = 1/2$) with FEC and SDD for signals transmitted over a Nakagami fading channel ($m = 1$) with pulsed-noise jamming (SNR $= 16$ dB).

cation system not employing FEC and SDD, as was shown in Figure 7. However, for the IEEE 802.11a wireless local area network standard, FEC with SDD is specified.

To examine the effect of the Nakagami fading channel, we examine Figure 10, which demonstrates system performance for different values of the m parameter. Based on the findings from the two previous figures, where the worst-case scenario for the receiver is for $p = 1$, we plot the probability of bit error only for continuous noise jamming. Initially, we observe that, as m increases, the performance of the receiver improves. As m approaches infinity, the performance approaches the AWGN limit. The difference in performance for small values of SIR is minor. In other words, when the jamming power is large, the fading conditions play a minor role. Conversely, as SIR increases and we encounter small jamming power, the results are the opposite. For large SIR, the fading conditions determine to a large extent the overall performance. A small increase of m from 1/2 to 1 improves the bit error rate by a magnitude of 10^{-3} when $\text{SNR} = 10\,\text{dB}$.

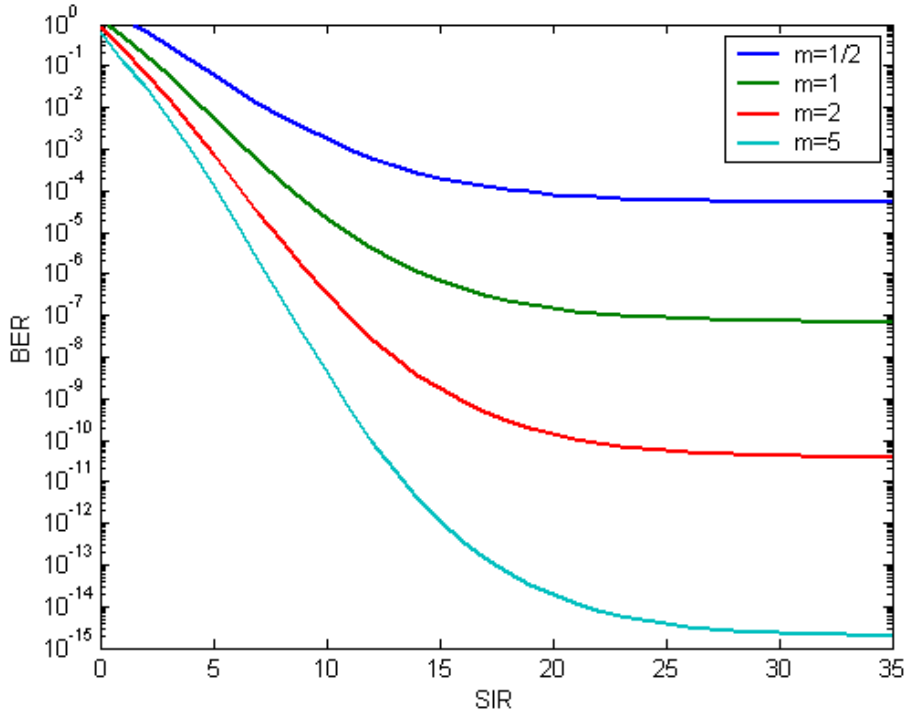

Figure 10. BPSK/QPSK ($r = 1/2$) with FEC and SDD over a Nakagami fading channel with continuous noise jamming ($\text{SNR} = 10\,\text{dB}$).

The next plots show the difference in performance introduced by changing the code rate. Here, we use $r = 3/4$, specified for data rates of nine Mbps (BPSK) and 18 Mbps (QPSK). In Figure 11 we see the performance for $m = 1$ and $\mathrm{SNR} = 10\,\mathrm{dB}$, while in Figure 12 we have increased the signal-to-noise ratio to 16 dB. The general characteristics observed for the $r = 1/2$ code are repeated when a $r = 3/4$ code is used. To compare the performance obtained with the two codes, in Figure 13 the performance for both $r = 1/2$ and $r = 3/4$ codes with continuous noise jamming are plotted. Generally, when the code rate is large, we get higher data rates. Alternatively, if we are satisfied with the data rate, we may reduce the coded bit duration and achieve less bandwidth expansion. On the other hand, we lose in performance when we use a higher code rate.

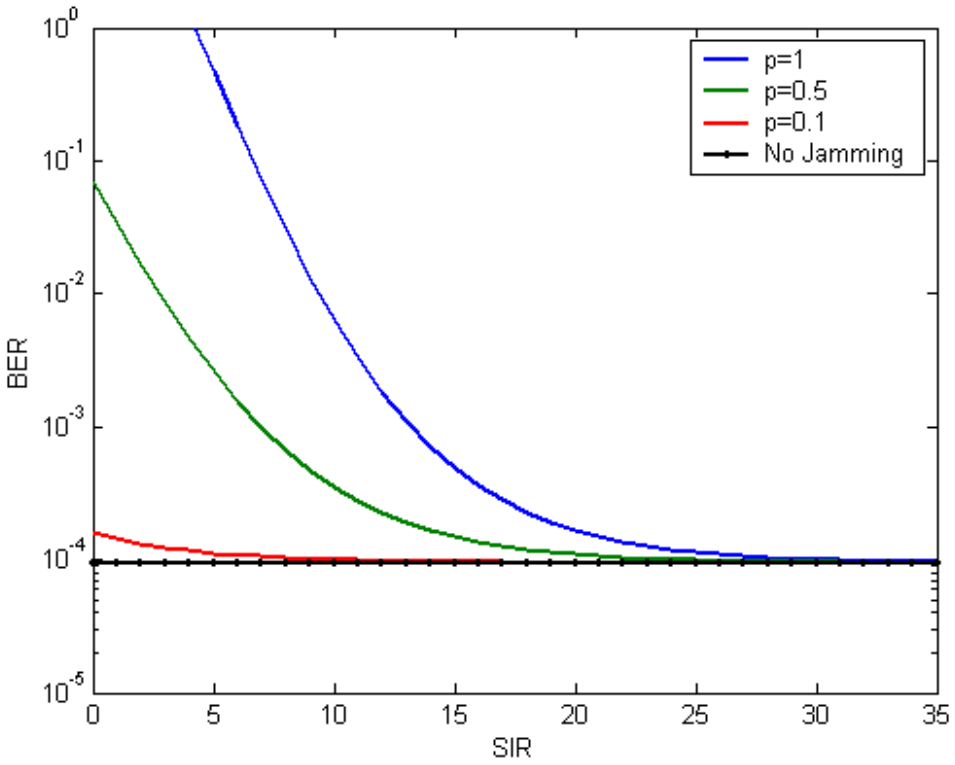

Figure 11. BPSK/QPSK ($r = 3/4$) with FEC and SDD over a Nakagami fading channel ($m = 1$) with pulsed-noise jamming ($\mathrm{SNR} = 10\,\mathrm{dB}$).

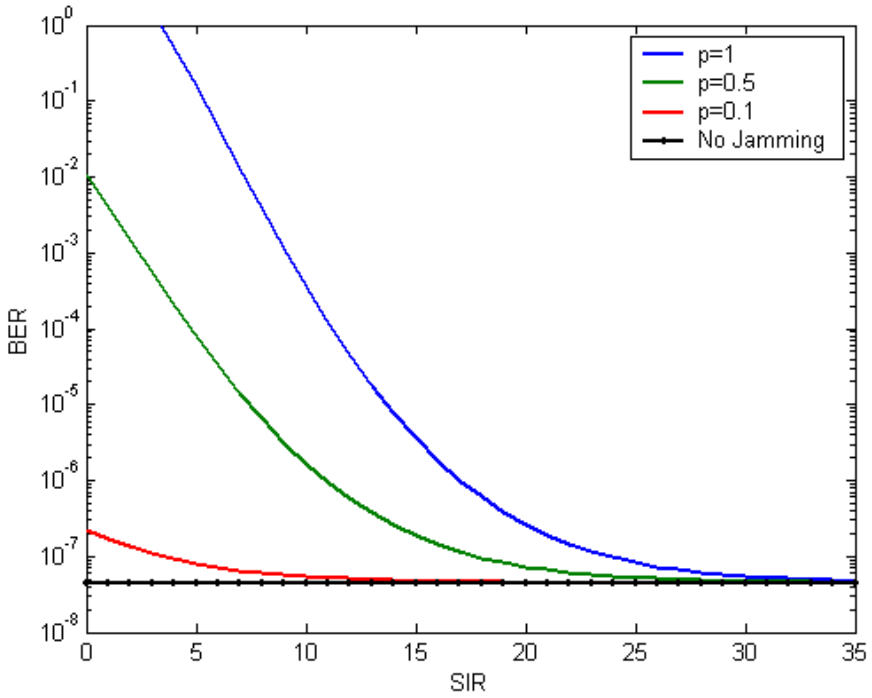

Figure 12. BPSK/QPSK ($r = 3/4$) with FEC and SDD over a Nakagami fading channel ($m = 1$) with pulsed-noise jamming (SNR $= 16$ dB).

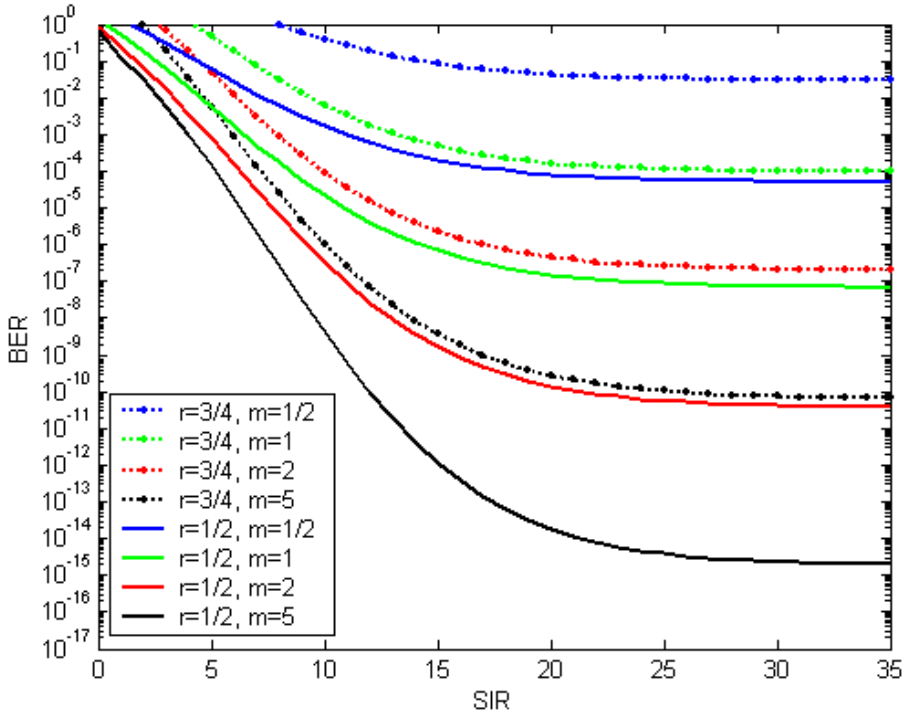

Figure 13. BPSK/QPSK ($r = 3/4$) vs. $r = 1/2$ with FEC and SDD over a Nakagami fading channel with continuous noise jamming (SNR $= 10$ dB).

In order to gain some perceptive on the performance improvement, in Figures 14 and 15, we compare BPSK/QPSK transmitted over a Nakagami fading channel in the presence of pulsed-noise jamming with and without FEC and SDD. In Figure 14, for $r = 1/2$ and $\text{SNR} = 10\,\text{dB}$, FEC with SDD provides significant performance improvement. The advantages depending on m begin at different SIR. For $m = 1/2$, FEC with SDD is better for values of SIR larger than four dB, while for $m = 5$ the corresponding value is around 2 dB.

In Figure 15 the code rate is $r = 3/4$ and the overall performance is poorer than $r = 1/2$. The cross-over point where the coding gain is positive after 15 dB ($m = 1/2$) and four dB ($m = 5$), respectively. Finally, it is remarkable that the nominal $P_b = 10^{-4}$ cannot be achieved without coding even when the fading conditions are light ($m = 5$) for $\text{SNR} = 10\,\text{dB}$. On the other hand, FEC and SDD makes this feasible even under the severest fading conditions.

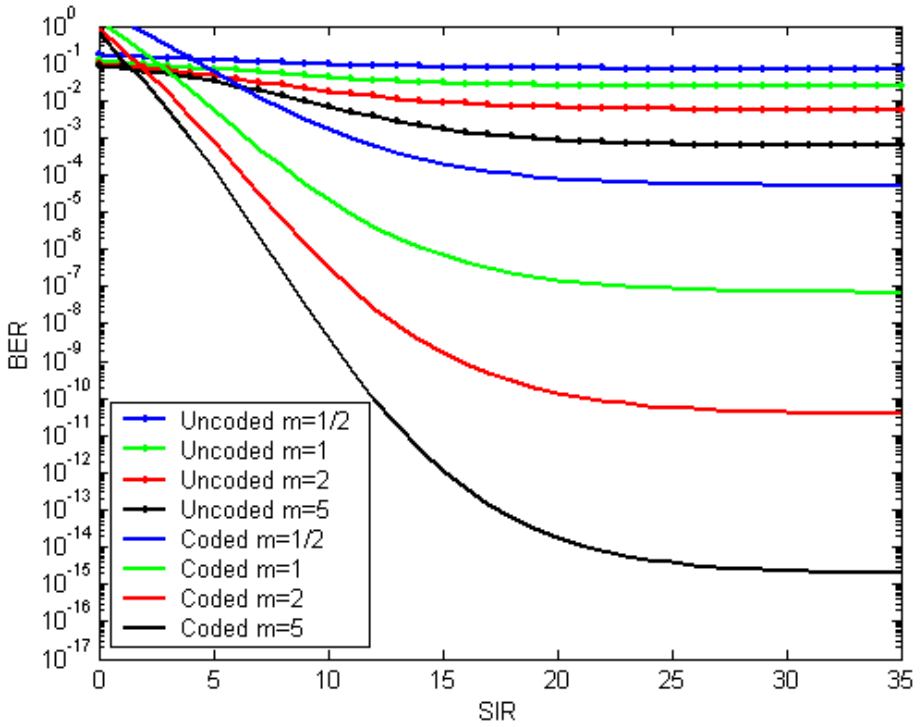

Figure 14. BPSK/QPSK ($r = 1/2$) with FEC and SDD over a Nakagami fading channel with continuous noise jamming ($\text{SNR} = 10\,\text{dB}$) vs. uncoded performance.

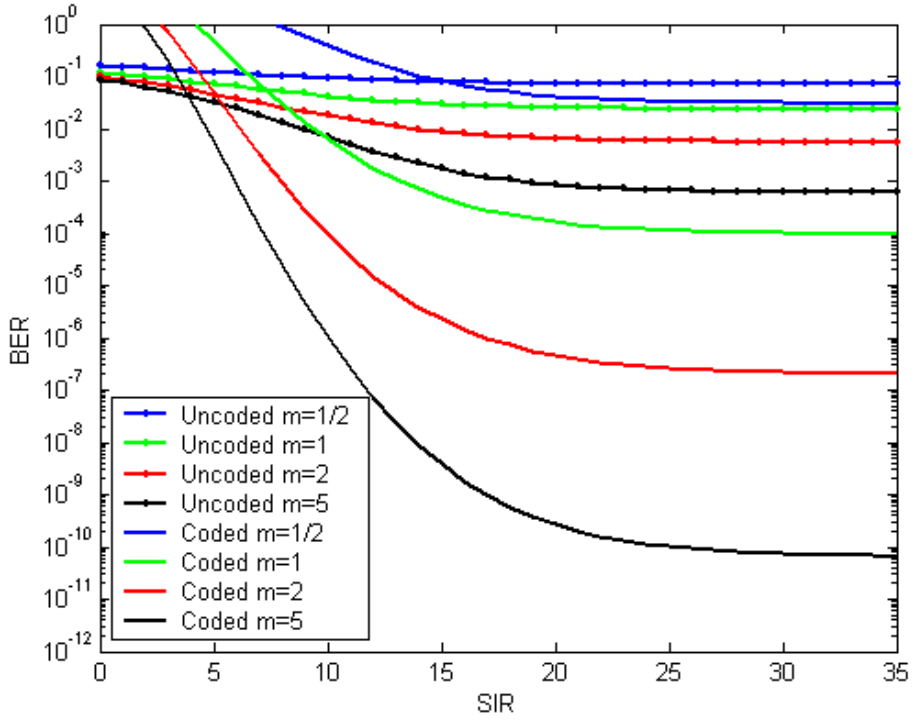

Figure 15. BPSK/QPSK ($r = 3/4$) with FEC and SDD over a Nakagami fading channel with continuous noise jamming ($\mathrm{SNR} = 10\,\mathrm{dB}$) vs. uncoded performance.

C. 16QAM/64QAM

The bandwidth efficient M-ary QAM is used for even higher data rates between 24 and 54 Mbps.

1. Without FEC and SDD

For a second time we borrow the results from [4], and we present results that verify the same general trend of improved performance for higher values of m. Again, we use the usual range of 1/2 to 5 for m and assume the jammer is on for 50% of the time ($p = 0.5$). In Figure 16 for 16QAM we have a poorer bit error rate as compared to Figure 5 for BPSK and QPSK. As expected, 16QAM performs better than 64QAM, and a larger signal-to-noise ratio ($\mathrm{SNR} = 20\,\mathrm{dB}$) is used for the 64QAM signal performance shown in Figure 17.

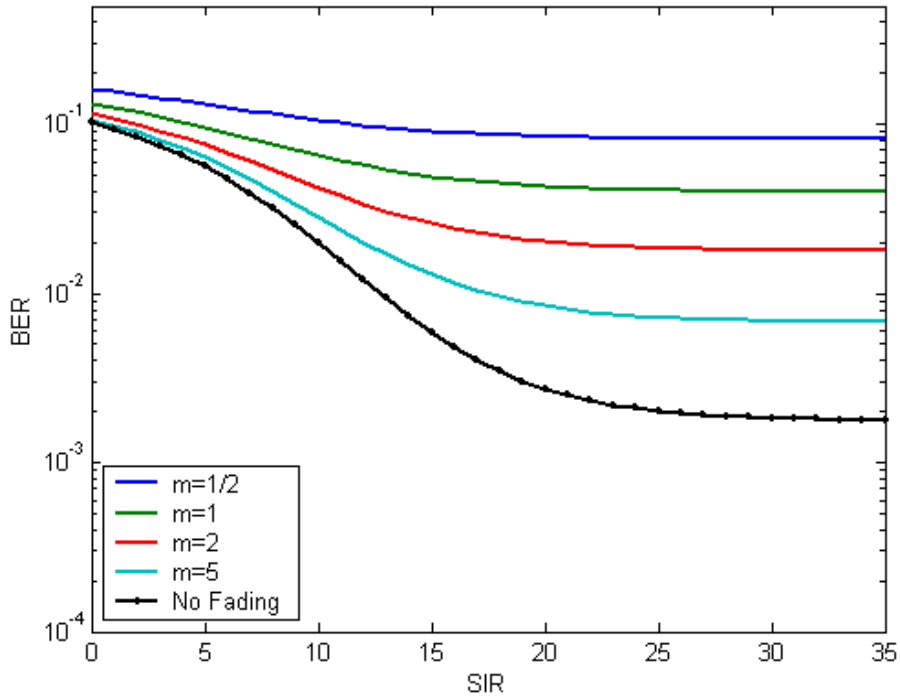

Figure 16. 16QAM transmitted over a Nakagami fading channel with pulsed-noise jamming, SNR = 10 dB, and $p = 0.5$ [After Ref. 4.].

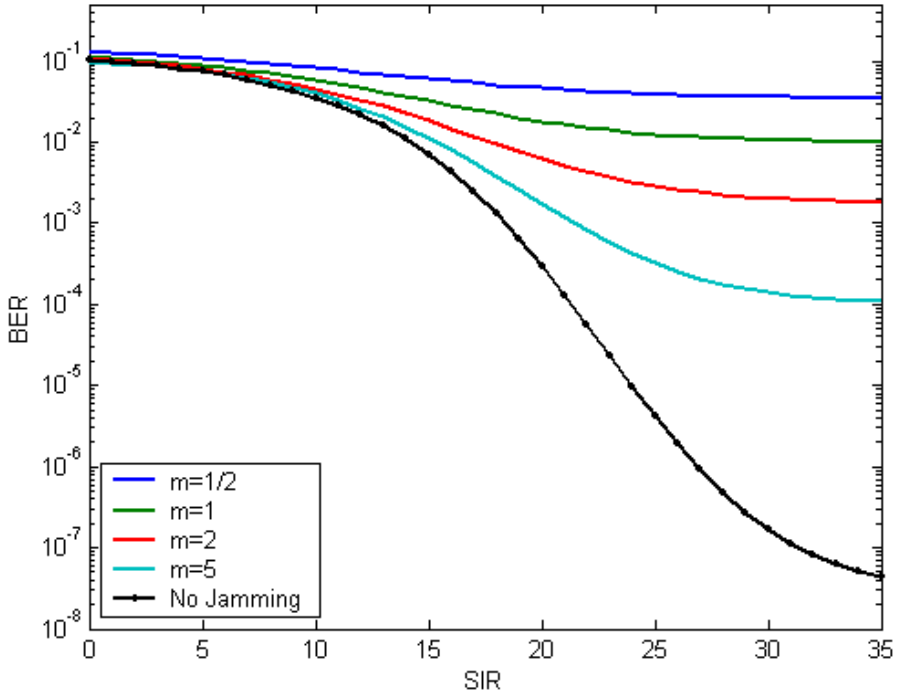

Figure 17. 64QAM transmitted over a Nakagami fading channel with pulsed-noise jamming, SNR = 20 dB, and $p = 0.5$ [After Ref. 4.].

2. With FEC and SDD

The approach followed for the SDD demodulation for BPSK with FEC does not apply for the MQAM case. Demodulating a binary signal with SDD means that the demodulator output is non-binary. Using a metric that provides enough resolution to separate the various levels, like the Euclidean distance, the decoder decides which path is correct. When non-binary modulation is used, we cannot do the same. As a result, we assume that the quantization is applied to the demodulated symbols. During the conversion from symbol to bit, the resulting bits inherit the quantized level of the parent symbol. Moreover, the process of deinterleaving spreads the bits in time, and we can reasonably continue our analysis based on the approach for binary signals.

The main difference we should bear in mind is to use the proper formula for the probability of bit error for M-ary QAM in Equation (3.9). According to [9], the probability of bit error in AWGN for square M-ary QAM constellations is

$$P_b = \frac{4(M-1)}{q\sqrt{M}} Q\left(\sqrt{\frac{3q\,\mathrm{SNR}}{M-1}}\right), \tag{3.52}$$

where q is the number of bits per symbol, and M is the number of possible combinations of q bits. The relation between q and M is $q = \log_2 M$. By analogy with Equation (3.9), valid for BPSK with FEC and SDD, we get

$$P_d = \frac{4(M-1)}{q\sqrt{M}} Q\left(\sqrt{\frac{3q\left(\sum_{l=1}^{i} a_{c_l}^2/\sigma_t^2 + \sum_{l=i+1}^{d} a_{c_l}^2/\sigma_o^2\right)}{M-1}}\right). \tag{3.53}$$

Following the methodology used for BPSK and setting $M = 16$ and $q = 4$, we get Figures 18, 19, and 20 for 16QAM. In Figures 18 and 19 the signal experiences Rayleigh fading for different values of p. Next, in Figure 20 the jamming is continuous, and we again use the range for m (1/2, 5). As expected, the performance is worse than for BPSK, but now data rate is higher. For $r = 1/2$ with 16QAM, we have 24 Mbps, while for $r = 3/4$ with 16QAM, we get 36 Mbps.

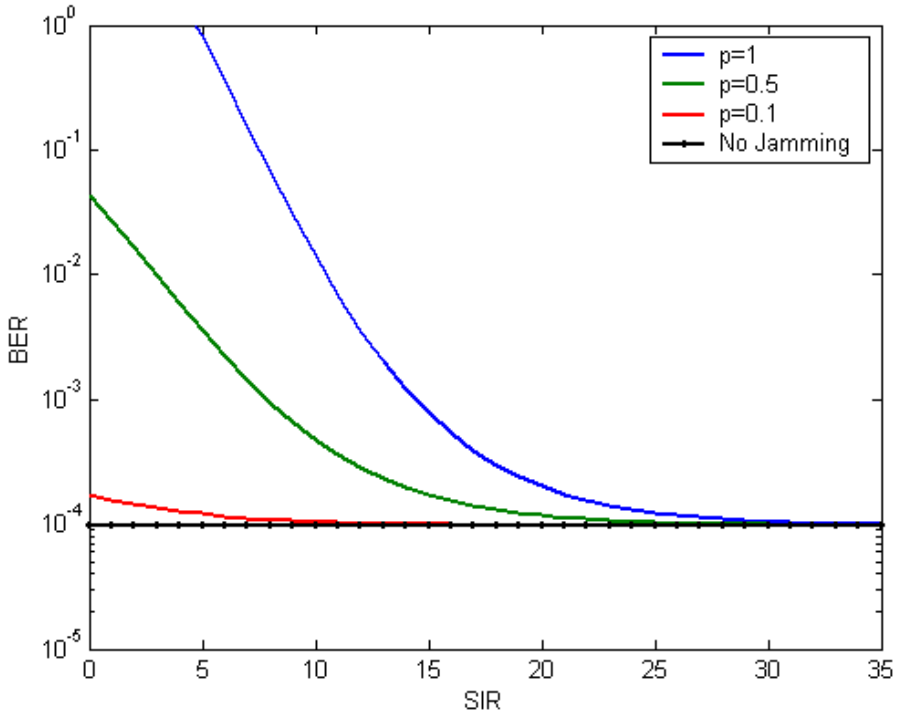

Figure 18. 16QAM ($r = 1/2$) with FEC and SDD transmitted over a Nakagami fading channel ($m = 1$) with pulsed-noise jamming (SNR $= 10$ dB).

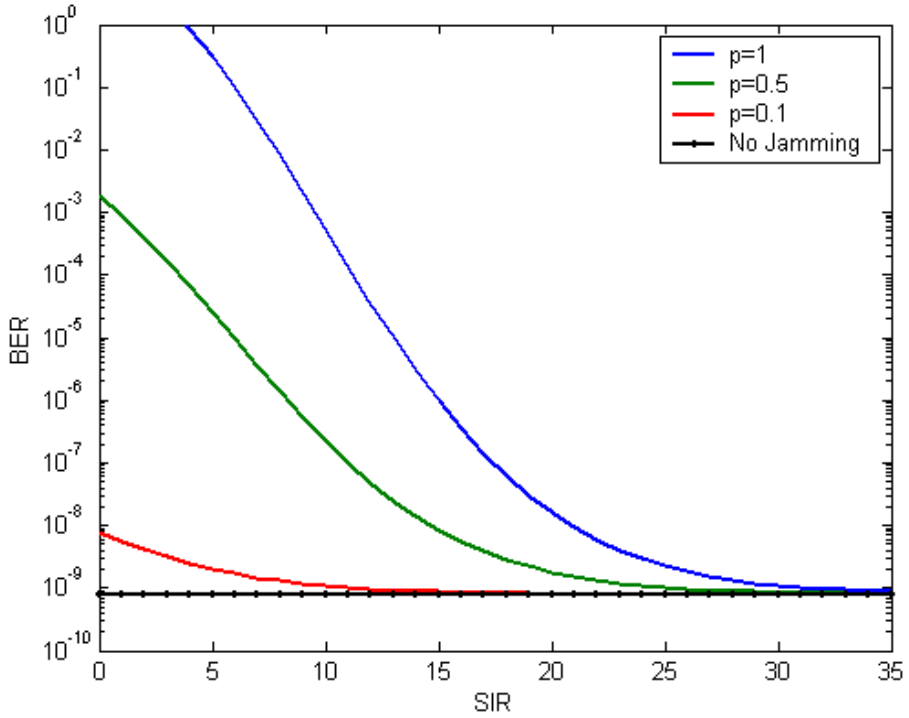

Figure 19. 16QAM ($r = 1/2$) with FEC and SDD transmitted over a Nakagami fading channel ($m = 1$) with pulsed-noise jamming (SNR $= 16$ dB).

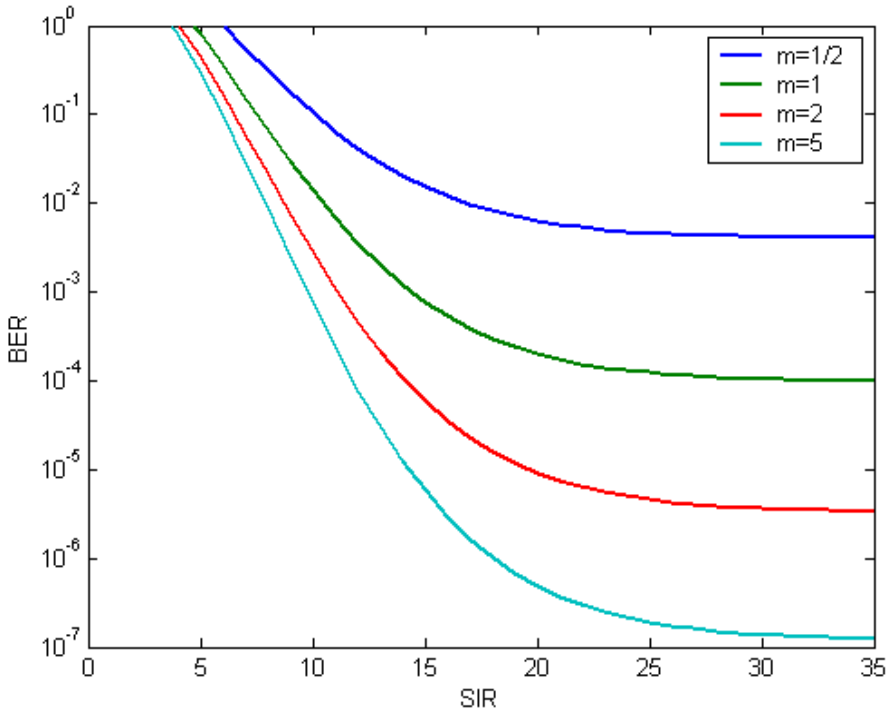

Figure 20. 16QAM ($r = 1/2$) with FEC and SDD transmitted over a Nakagami fading channel with continuous noise jamming ($\text{SNR} = 10\,\text{dB}$).

The necessary alterations of Equation (3.53) for 64QAM, the last modulation technique we are examining, is to set $M = 64$ and $q = 6$. Again, we achieve higher data rates, but the performance is even worse compared to all previous cases. For $r = 2/3$ with 64QAM we have 48 Mbps, while for $r = 3/4$ with 64QAM we get 54 Mbps. In Figure 21 we see the probability of bit error for $r = 3/4$. The combination of 64QAM and the larger value of the possible code rates has the poorest performance and will be used only in very favorable conditions of fading and signal-to-noise ratio. That is the reason we use the relatively high value of $\text{SNR} = 26\,\text{dB}$.

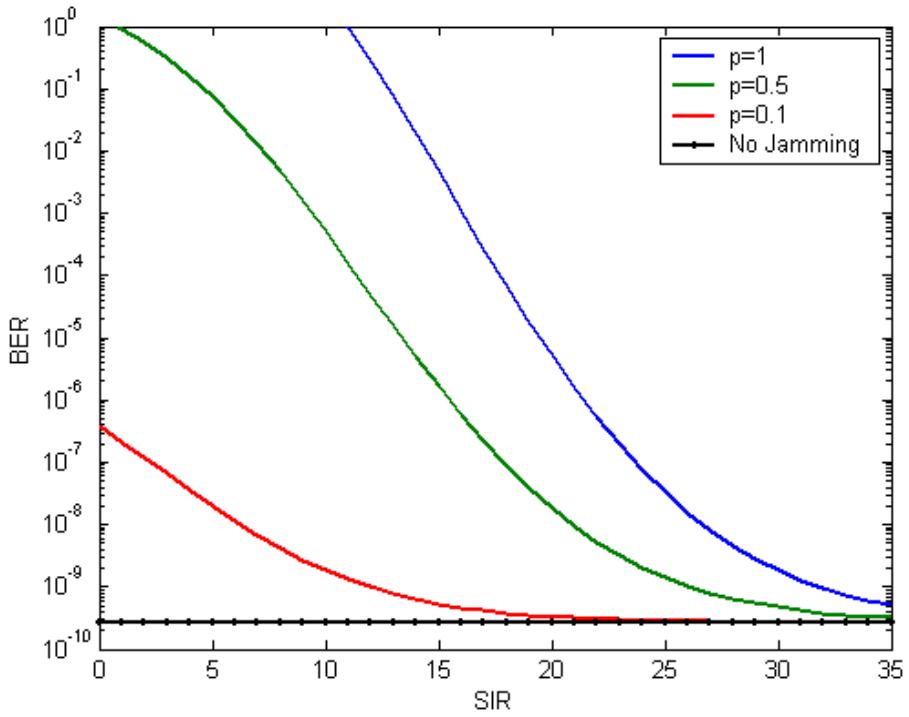

Figure 21. 64QAM ($r = 3/4$) with FEC and SDD transmitted over a Nakagami fading channel with $m = 1$ (Rayleigh fading), and $\text{SNR} = 26\,\text{dB}$.

D. OFDM SYSTEM PERFORMANCE

Having investigated the performance of every combination of modulation and code rate utilized by the IEEE 802.11a standard, we now examine the other significant characteristic of the IEEE 802.11a waveform, orthogonal frequency-division multiplexing (OFDM). We consider that all 48 data sub-carriers are transmitted parallel. It is likely that each sub-carrier may encounter different fading. The question that rises is how shall we handle and combine the bit error rate of each sub-carrier that was derived in the previous sections.

We answer that question by sharing the approach of [3] and [4]. Since the IEEE 802.11a is a protocol for WLAN indoor transmission, by default the fading environment is a variable one. Open or closed doors contribute greatly to that variability. Multiple reflections on the walls and the objects of a room are also responsible. Additionally, there are other diffraction and scattering factors that obviously affect an indoor communication link.

The Nakagami distribution is a great aide in our effort, because by changing the m parameter we model different fading channels. Supposing that both severe and mild fading conditions are likely to occur simultaneously for different sub-carriers, we treat each sub-carrier as being independent and subject to Nakagami fading with different m. Assuming that all values of m are probable in a specific range, we model m as a uniformly distributed random variable. Ranging m from 1/2 to 5 is a reasonable assumption, and we must calculate the bit error rate 48 times and take the average.

1. BPSK/QPSK

The results for the uncoded signal are presented in [4]. In Figure 22 we can see the difference of the combined OFDM signal, compared to a single BPSK/QPSK with FEC and SDD. We plot the bit error rate against the extremes of m (1/2, 5). The overall picture we get is the domination of the severe fading in the combined signal. This finding is confirmed in Figure 23 where we have increased SNR to 16 dB. The performance trend for the average of the 48 sub-carriers is closer to the $m = 1/2$ curve for most values of SIR.

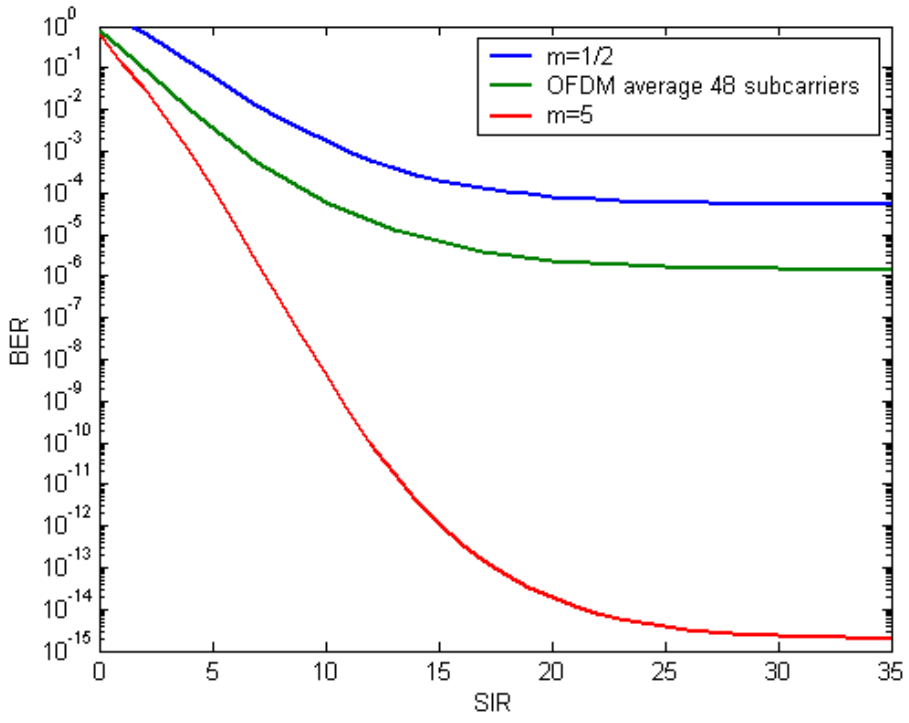

Figure 22. OFDM BPSK ($r = 1/2$) with FEC and SDD (SNR = 10 dB).

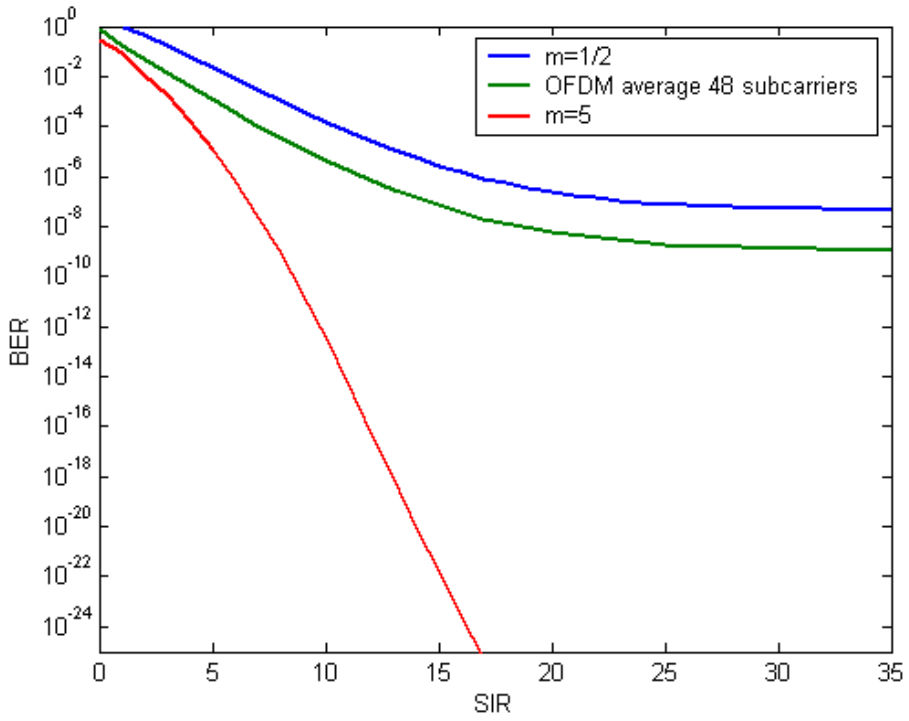

Figure 23. OFDM BPSK ($r = 1/2$) with FEC and SDD (SNR = 16 dB).

The difference between the bit error rate for the single signal with $m = 1/2$ and the OFDM signal is nearly constant for every SIR. Of course the bit error rate for OFDM is smaller by a factor of 10^{-2}. However, when the jamming power is strong, the OFDM signal appears to be closer to the curve for $m = 5$.

2. 16QAM/64QAM

For the M-ary QAM signal, the combined signal exhibits the same characteristics. In Figures 24 and 25 we plot 16QAM performance for different code rates and signal-to-noise ratios. The curve of the combined signal seems even closer to the one for $m = 1/2$. However, for SIR less than 10 dB the OFDM signal performs like the single carrier experiencing light fading conditions ($m = 5$). Due to limitations of the software used for the generation of the plots, we cannot obtain results for the 64QAM signal.

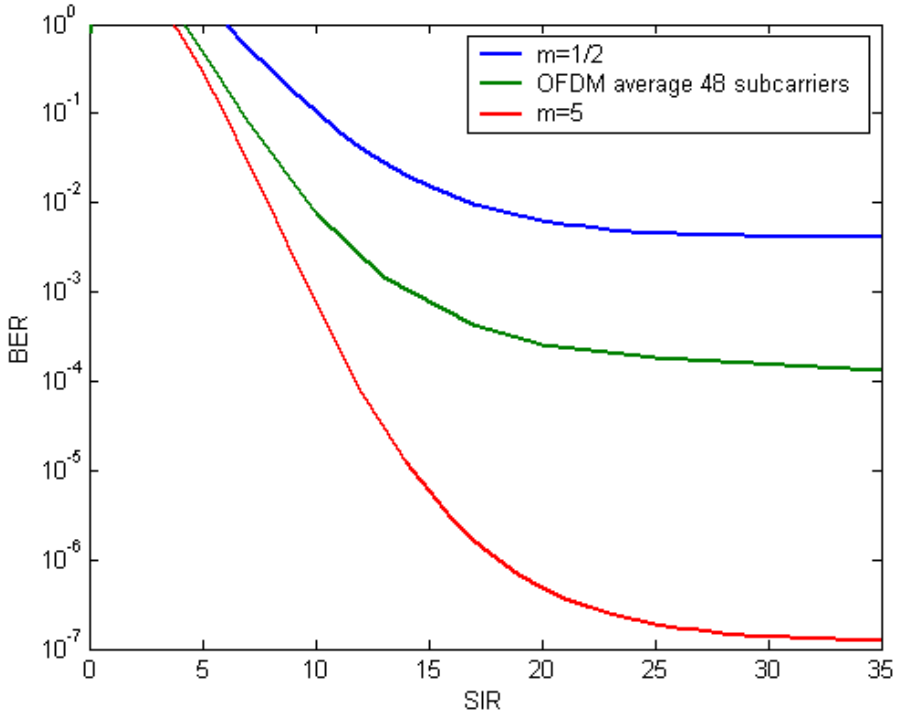

Figure 24. OFDM 16QAM ($r = 1/2$) with FEC and SDD (SNR = 10 dB).

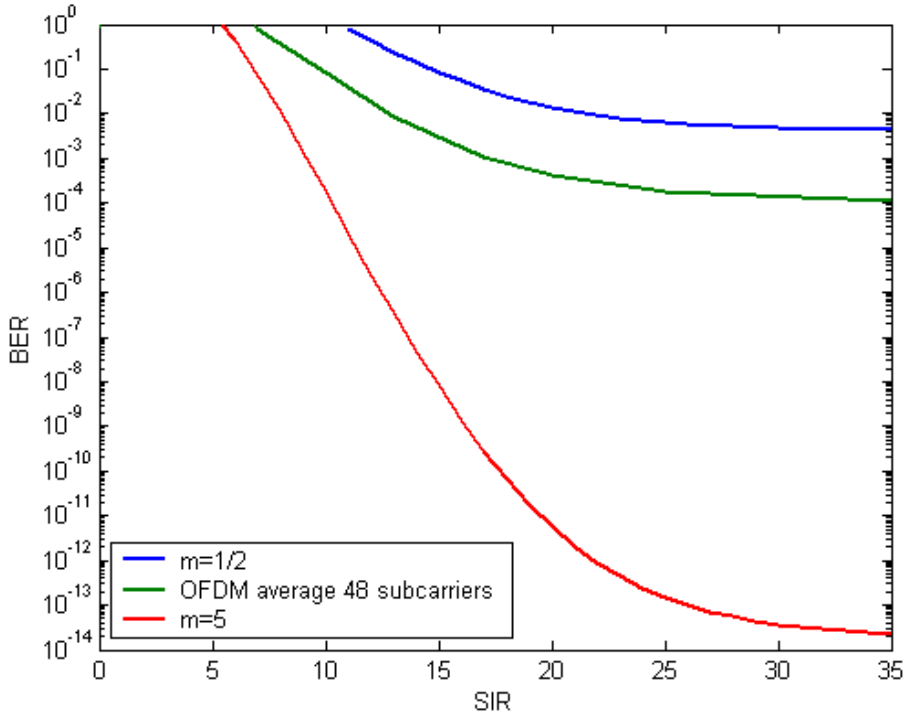

Figure 25. OFDM 16QAM ($r = 3/4$) with FEC and SDD (SNR = 16 dB).

E. SUMMARY

This chapter presented the effect of fading and pulsed-noise jamming on the signal. The comparison between coded and uncoded performance is essential to establish the importance of convolutional coding to reliable communication. We plotted the results for various combinations of modulations and code rates. As the code rate increases, which means that the coded signal has less redundancy, we confirmed the results of [4] regarding the deterioration of the bit error rate. By changing parameter p, we determined that continuous jamming is most effective against FEC and SDD for the maximum-likelihood receiver. Variations of the m parameter gave insight as to how severe the effect of fading is for $m = 1/2$ compared to larger values of m.

In the last part, we dealt with the combined OFDM signal with FEC and SDD. Based on the assumption that all sub-carriers are likely to experience different fading conditions, we randomly assigned values for m in the region 1/2 to 5. For all modulations the domination of the smallest m was obvious, which agreed with the findings for uncoded OFDM after Ref [4].

Up to this point we have assumed the jamming signal does not experience any kind of fading. This is close to reality for an airborne jammer who enjoys LOS with the jammed receiver. The question that rises is what is the effect when the jammer does encounter fading, and this is discussed in the next chapter.

IV. PERFORMANCE ANALYSIS WITH FEC AND SDD, NAKAGAMI FADING CHANNELS, AND FADED PULSED-NOISE JAMMING

A. INTRODUCTION

Having examined the performance of a system designed to receive an IEEE 802.11a waveform transmitted over a Nakagami fading channel with pulsed-noise jamming, we now proceed to evaluate the communications system performance when the jamming signal also experiences fading. In this case the noise power of the jammer σ_j^2 is no longer constant but must be modeled as a random variable. The probability of bit error is now conditional on the noise power of the jammer. Since we assume a Nakagami fading channel, σ_j^2 is modeled as a Nakagami-squared random variable. This chapter is organized like the previous one in order to make comparison with previous results easier.

B. BPSK/QPSK

1. Without FEC

In [14] the probability bit error for BPSK/QPSK with noise jamming is given as

$$P_b = Q\left(\sqrt{2\frac{a_c^2}{\sigma_j^2 + \sigma_o^2}}\right) \tag{4.1}$$

where $\sigma_j^2 + \sigma_o^2$ represents the power of additive, Gaussian noise. As mentioned previously, σ_j^2 is modeled as a random variable. As a result, Equation (4.1) is now a conditional probability. To get the unconditional P_b, we first need to find the pdf corresponding to the argument of the Q-function, $a_c^2/\left(\sigma_j^2 + \sigma_o^2\right)$. This pdf is extremely complex and, in order to simplify the analysis, we assume that the power of the AWGN σ_o^2 is negligible compared to σ_j^2. This is true for most values of SIR when SNR is large. Now the probability of bit error simplifies to

$$P_b = Q\left(\sqrt{2\frac{a_c^2}{\sigma_j^2}}\right). \tag{4.2}$$

To continue our analysis, we define

$$t = \frac{a_c^2}{\sigma_j^2} = \frac{x}{y}, \tag{4.3}$$

which means that P_b is now conditional on the random variable t

$$P_b(t) = Q\left(\sqrt{2t}\right). \tag{4.4}$$

Both x and y are independent, Nakagami-squared random variables and, by using the pdf of a Nakagami-squared random variable obtained in [3] and adjusting it for our notation, we have

$$f_X(x) = \frac{1}{\Gamma(m_s)}\left(\frac{m_s}{\overline{x}}\right)^{m_s} x^{m_s-1} e^{-\frac{m_s x}{\overline{x}}} \tag{4.5}$$

$$f_Y(y) = \frac{1}{\Gamma(m_j)}\left(\frac{m_j}{\overline{y}}\right)^{m_j} y^{m_j-1} e^{-\frac{m_j y}{\overline{y}}} \tag{4.6}$$

where $\overline{x}$ is the average power of the received information signal, and $\overline{y}$ is the average power of the jamming signal. The new parameters m_s and m_j are the Nakagami parameters for the fading channel of the desired and the jamming signal, respectively.

As we find in [15], the pdf of the ratio of two independent random variables is given by

$$f_T(t) = \int_0^\infty y\, f_X(ty) f_Y(y)\, dy\,. \tag{4.7}$$

If we substitute Equations (4.5) and (4.6) into Equation (4.7), we get

$$f_T(t) = \int_0^\infty y \frac{1}{\Gamma(m_s)}\left(\frac{m_s}{\overline{x}}\right)^{m_s} (ty)^{m_s-1} e^{-\frac{m_s ty}{\overline{x}}} \frac{1}{\Gamma(m_j)}\left(\frac{m_j}{\overline{y}}\right)^{m_j} y^{m_j-1} e^{-\frac{m_j y}{\overline{y}}}\, dy \tag{4.8}$$

which can be manipulated to give

$$f_T(t) = \frac{1}{\Gamma(m_s)\Gamma(m_j)} \left(\frac{m_s}{\overline{x}} \right)^{m_s} \left(\frac{m_j}{\overline{y}} \right)^{m_j} t^{m_s - 1} \int_0^\infty y^{m_s + m_j - 1} e^{-y\left(\frac{m_s t}{\overline{x}} + \frac{m_j}{\overline{y}} \right)} dy \,. \tag{4.9}$$

From [16] we use the identity

$$\int_0^\infty x^{\nu-1} e^{-\mu x} dx = \frac{1}{\mu^\nu} \Gamma(\nu), \quad \{\mathrm{Re}(\mu) > 0, \mathrm{Re}(\nu) > 0\}. \tag{4.10}$$

Setting

$$\nu = m_s + m_j \tag{4.11}$$

and

$$\mu = \frac{m_s t}{\overline{x}} + \frac{m_j}{\overline{y}}, \tag{4.12}$$

we can use (4.10) to evaluate (4.9) with the result

$$f_T(t) = \frac{1}{\Gamma(m_s)\Gamma(m_j)} \left(\frac{m_s}{\overline{x}} \right)^{m_s} \left(\frac{m_j}{\overline{y}} \right)^{m_j} t^{m_s - 1} \frac{1}{\left(\frac{m_s t}{\overline{x}} + \frac{m_j}{\overline{y}} \right)^{m_s + m_j}} \Gamma(m_s + m_j). \tag{4.13}$$

Rearranging terms and expressing the second part in terms of SIR, where

$$\mathrm{SIR} = \frac{\overline{x}}{\overline{y}}, \tag{4.14}$$

we obtain to the pdf of the ratio of two Nakagami-squared random variables as

$$f_T(t) = \frac{\Gamma(m_s + m_j)}{\Gamma(m_s)\Gamma(m_j)} \left(\frac{m_s}{m_j} \right)^{m_s} t^{m_s - 1} \frac{\mathrm{SIR}^{m_j}}{\left(\frac{m_s}{m_j} t + \mathrm{SIR} \right)^{m_s + m_j}}. \tag{4.15}$$

An alternative derivation of Equation (4.15) is given in [6].

To obtain the unconditional P_b, we must integrate the product of the conditional $P_b(t)$ and the probability density function $f_T(t)$ over the values for which t is valid:

$$P_b = \int_0^{\infty} P_b(t) f_T(t)\, dt\,. \tag{4.16}$$

Equation (4.16) must be evaluated numerically. The following four figures amply demonstrate the effect of fading upon the jamming signal. First, in Figure 26 we examine the case for the most unfavorable fading of the desired signal ($m_s = 1/2$). The faded jamming signal improves the performance of the system. For light fading of the jamming signal ($m_j = 5$), performance approaches that of non-faded jamming. For values of $m_j < 5$, performance improves as m_j gets smaller. At the extreme of $m_j = 1/2$, we find an overall improvement of two dB relative to the unfaded jamming signal performance. What is equally important is the fact that the curves exhibit the same behavior for all values of SIR. All curves exhibit the same characteristics and are essentially parallel to each other. This behavior is independent of the SIR.

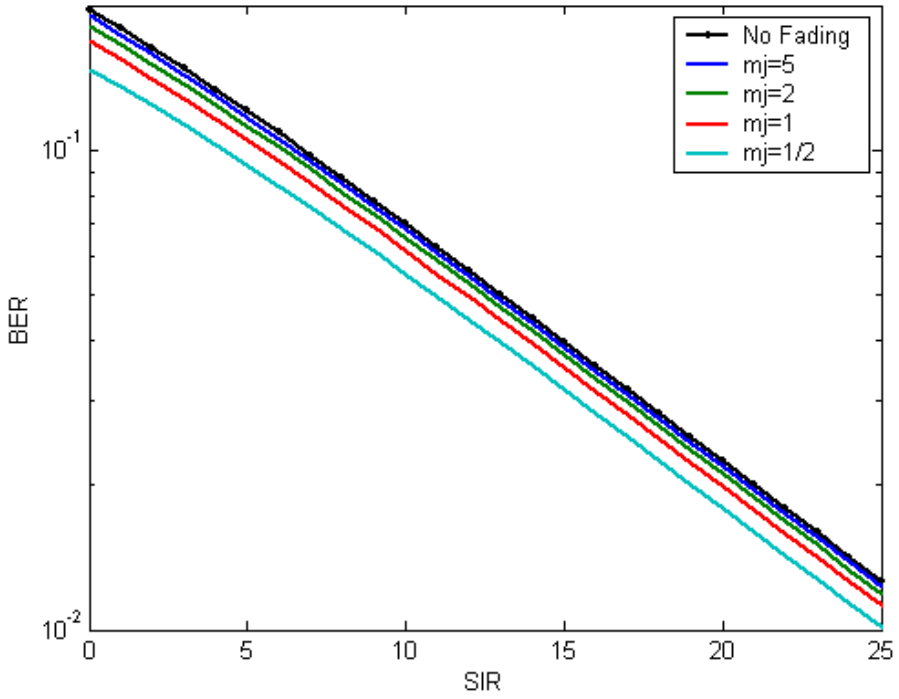

Figure 26. Performance of BPSK/QPSK ($m_s = 1/2$) when the jamming signal experiences Nakagami fading.

Continuing with Figure 27, we examine improved fading conditions of the desired signal and consider Rayleigh fading ($m_s = 1$). Again in this case we can see that the larger the value of m_j, the smaller the improvement of the probability of bit error relative to no-fading of the jamming signal. However, this improvement is not independent of SIR. Again, we identify a maximum difference of two dB, but that is true only for very small values of SIR. As the value of SIR grows, we note that the curves converge. When the information signal power increases, fading of the jamming signal has little effect, whereas it has virtually no effect for values of SIR over 12 dB.

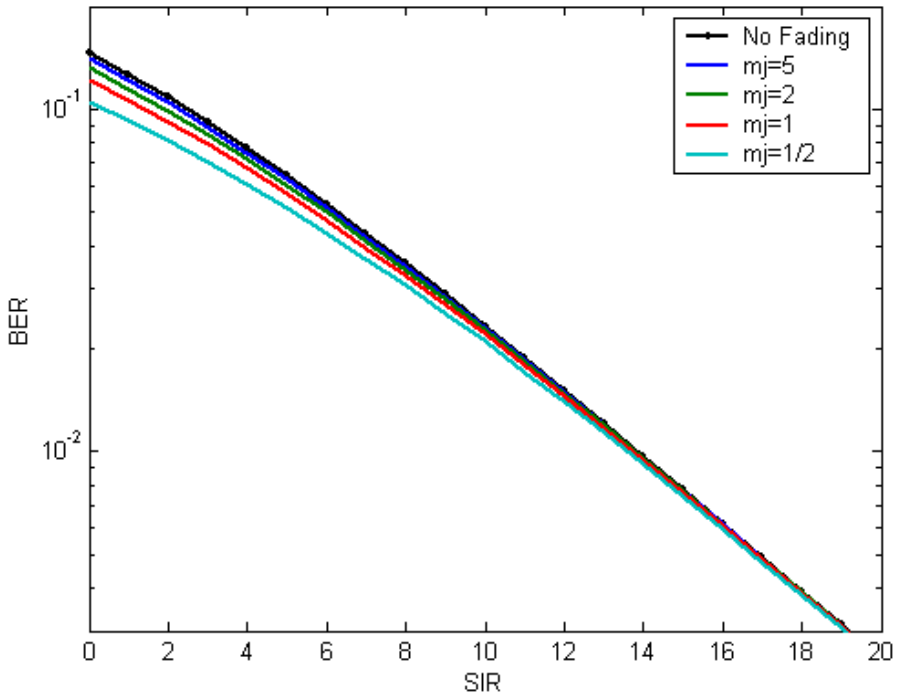

Figure 27. Performance of BPSK/QPSK ($m_s = 1$) when the jamming signal experiences Nakagami fading.

Figures 28 and 29 reveal a different effect. We again increase m_s, simulating lighter fading. In this case the improvement we saw earlier as m_j decreases still holds only for very small SIR. For large SIR we observe that fading of the jammer degrades the bit error rate compared to unfaded jamming. In Figure 28, SIR = 5.3 dB is the crossover point, while in Figure 29 the corresponding value is 3.7 dB. That point where the curves

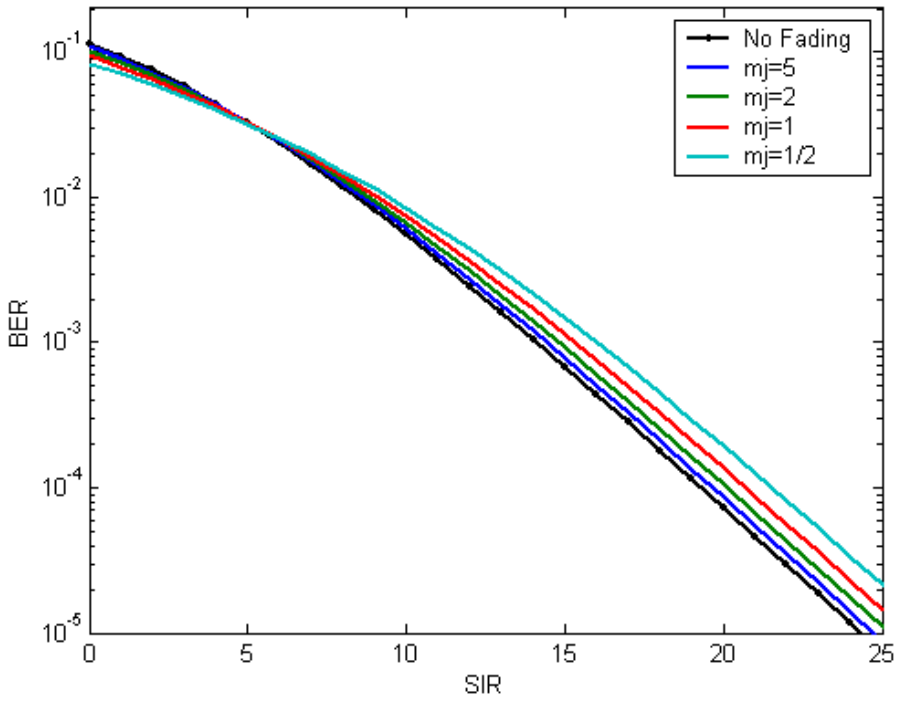

Figure 28. Performance of BPSK/QPSK ($m_s = 2$) when the jamming signal experiences Nakagami fading.

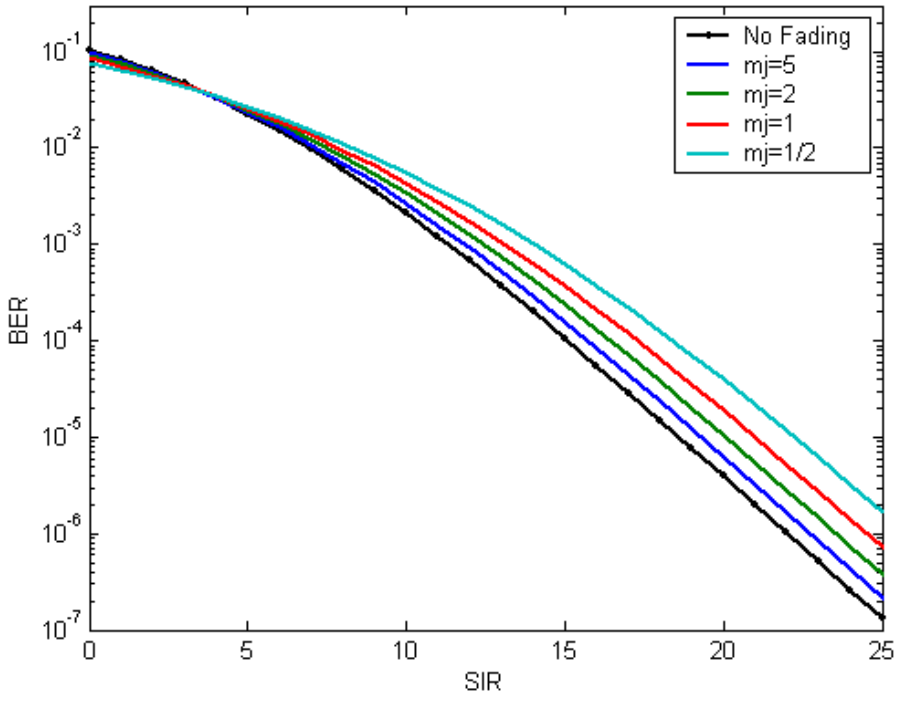

Figure 29. Performance of BPSK/QPSK ($m_s = 3$) when the jamming signal experiences Nakagami fading.

cross each other exists for all values of $m_s > 1$. In Table 3 we see how the crossover point decreases as the fading of the information signal gets lighter.

Table 3. Crossover point of curves for different m_s.

m_s	1.5	1	1.2	1.5	2	2.5	3	3.5	4	4.5	5	8
SIR (dB)	N/A	N/A	10.5	7.4	5.3	4.5	3.7	3.5	3.2	3	2.7	2.3

2. With FEC and SDD

The analysis for a system with FEC and SDD when the jamming signal experiences fading is the same as in Chapter III up to Equation (3.8). From that point and on, when σ_j^2 is modeled as a random variable, we continue by splitting the sum of $a_{c_l}^2 / \sigma_j^2$ over the d bits as follows:

$$P_d = Q\left(\sqrt{2\sum_{l=1}^{d}\frac{a_{c_l}^2}{\sigma^2}}\right) = Q\left(\sqrt{2\left(\sum_{l=1}^{i}\frac{a_{c_l}^2}{\sigma_t^2} + \sum_{l=i+1}^{d}\frac{a_{c_l}^2}{\sigma_o^2}\right)}\right) \tag{4.17}$$

which is equivalent to

$$P_d = Q\left(\sqrt{2\left(\sum_{l=1}^{i}\frac{a_{c_l}^2}{\sigma_j^2+\sigma_o^2} + \frac{1}{\sigma_o^2}\sum_{l=i+1}^{d}a_{c_l}^2\right)}\right). \tag{4.18}$$

Comparing Equations (3.9) and (4.18), we see that in the latter the power of the jamming signal σ_j^2 is not factored out of the sum of the i bits. Due to fading, σ_j^2 is in general different for every bit, and that detail complicates the analysis. Assuming $\sigma_j^2 \gg \sigma_o^2$, we obtain from Equation (4.18)

$$P_d = Q\left(\sqrt{2\left(\sum_{l=1}^{i}\frac{a_{c_l}^2}{\sigma_j^2} + \frac{1}{\sigma_o^2}\sum_{l=i+1}^{d}a_{c_l}^2\right)}\right). \tag{4.19}$$

By analogy with Chapter III, we define

$$h = \sum_{l=1}^{i} \frac{a_{c_l}^2}{\sigma_j^2} + \frac{1}{\sigma_o^2} \sum_{l=i+1}^{d} a_{c_l}^2 \ . \tag{4.20}$$

We note that P_d is conditioned on h and so is expressed as $P_d(h)$. To obtain the average P_d we must integrate the product of the conditional $P_d(h)$ and the probability density function of h ($f_H(h)$) over the values for which h is valid:

$$P_d = \int_0^\infty P_d(h) f_H(h)\, dh \,. \tag{4.21}$$

To find $f_H(h)$, we start by defining

$$h = w + h2 \tag{4.22}$$

where

$$w = \sum_{l=1}^{i} \frac{a_{c_l}^2}{\sigma_j^2} = \sum_{l=1}^{i} t \tag{4.23}$$

is the sum of i random variables t, and

$$h2 = \frac{1}{\sigma_o^2} \sum_{l=i+1}^{d} a_{c_l}^2 \tag{4.24}$$

is already defined in Chapter III.

Starting with the random variable w, we obtain its pdf by noting that it is the sum of i independent random variables t, where the probability density function of t is given in Equation (4.15). Due to the fact that $f_T(t)$ is too complex for our analysis to continue, we make the simplifying assumption that $m_s = 1$; that is, the desired signal's envelope obeys a Rayleigh distribution. Though this constrains our analysis, Rayleigh fading of the desired signal is very realistic for wireless applications since the Rayleigh distribution models severe fading conditions where there is no line-of-sight (LOS) signal path. Thus, Equation (4.15) simplifies to

$$f_T(t) = \frac{\Gamma(m_j + 1)}{\Gamma(m_j)} m_j{}^{m_j} \mathrm{SIR}^{m_j} \left(t + m_j \mathrm{SIR}\right)^{-m_j - 1} . \tag{4.25}$$

To continue with the calculation of $f_W(w)$, we again observe that w is the sum of i independent random variables. Instead of performing i convolutions of $f_T(t)$, which is straightforward conceptually but difficult in practice, we will exploit the Laplace transformation as in the previous chapter. In the Laplace domain, convolution corresponds to multiplication. We first Laplace transform $f_T(t)$ and then raise the result to the i^{th} power to account for the i independent random variables.

Hence,

$$\mathcal{L}\{f_T(t)\} = F_T(s) = \int_0^\infty f_T(t) e^{-st} dt . \tag{4.26}$$

Substituting Equation (4.25) into (4.26), we get

$$F_T(s) = \int_0^\infty \frac{\Gamma(m_j + 1)}{\Gamma(m_j)} m_j{}^{m_j} \mathrm{SIR}^{m_j} \left(t + m_j \mathrm{SIR}\right)^{-m_j - 1} e^{-st} dt \tag{4.27}$$

which can be written

$$F_T(s) = \frac{\Gamma(m_j + 1)}{\Gamma(m_j)} m_j{}^{m_j} \mathrm{SIR}^{m_j} \int_0^\infty \left(t + m_j \mathrm{SIR}\right)^{-m_j - 1} e^{-st} dt . \tag{4.28}$$

From [16] we know

$$\int_0^\infty (x + \beta)^\nu e^{-\mu x} dx = \mu^{-\nu - 1} e^{\beta\mu} \Gamma(\nu + 1, \beta\mu) . \tag{4.29}$$

Setting

$$x = t , \tag{4.30}$$

$$\beta = m_j \mathrm{SIR} , \tag{4.31}$$

$$\nu = -m_j - 1 , \tag{4.32}$$

and

$$\mu = s\,, \tag{4.33}$$

we can evaluate Equation (4.28) with (4.29) to obtain

$$F_T(s) = \frac{\Gamma(m_j + 1)}{\Gamma(m_j)} m_j{}^{m_j} \mathrm{SIR}^{m_j} s^{m_j} e^{m_j SIR s} \Gamma(-m_j, m_j \mathrm{SIR}\, s) \tag{4.34}$$

where $\Gamma(-m_j, m_j \mathrm{SIR}\, s)$ is the incomplete Gamma function [16].

Raising $F_T(s)$ to the i^{th} power, we find the Laplace transform of the pdf of the w random variable:

$$F_W(s) = \left(F_T(s)\right)^i = \left(\frac{\Gamma(m_j + 1)}{\Gamma(m_j)}\right)^i \left(m_j \mathrm{SIR}\right)^{m_j i} s^{m_j i} e^{m_j SIR s i} \left(\Gamma(-m_j, m_j \mathrm{SIR} s)\right)^i. \tag{4.35}$$

Now we must consider the random variable $h2$. Its pdf in the Laplace domain has already been calculated in Equation (3.31). Rewriting in terms of

$$\mathrm{SNR} = \frac{\overline{b_c}}{\sigma_o^2}\,, \tag{4.36}$$

we have

$$F_{H2}(s) = \frac{\mathrm{SNR}^{i-d}}{\left(s + \mathrm{SNR}^{-1}\right)^{(d-i)}}\,. \tag{4.37}$$

Now we obtain the Laplace transform of the pdf of the random variable h as

$$F_H(s) = F_W(s)\, F_{H2}(s)\,. \tag{4.38}$$

Substituting Equations (4.35) and (4.37) into (4.38), we get

$$F_H(s) = \left(\frac{\Gamma(m_j + 1)}{\Gamma(m_j)}\right)^i \left(m_j \mathrm{SIR}\right)^{m_j i} s^{m_j i} e^{m_j SIR s i} \left(\Gamma(-m_j, m_j \mathrm{SIR} s)\right)^i \frac{\mathrm{SNR}^{i-d}}{\left(s + \mathrm{SNR}^{-1}\right)^{(d-i)}}\,. \tag{4.39}$$

To find $\mathcal{L}^{-1}\{F_H(s)\}$ we again use the approach of Chapter III as expressed in Equation (3.44). Summarizing, we know both $f_H(h)$ and $P_d(h)$, the two terms in Equa-

tion (4.21), and we can calculate P_d numerically. As a final step, since everything is known in inequality (3.2), we can produce the necessary plots to illustrate our findings. An important point we must comment on is the assumption that AWGN on the jammed bits is negligible. Obviously, this assumption is plausible for large SNR and does not introduce any inaccuracies in this case. Of course, when SNR equals SIR the noise powers σ_o^2 and σ_j^2 are equal too. Such a situation violates our assumption and sets a constraint upon the range of SIR given a value of SNR for which our results are valid.

The question that begs an answer is how to set a threshold for the signal-to-interference ratio below which our results are valid, given a specific value of signal-to-noise ratio. In order to quantify when AWGN is negligible and our results are valid, we will ignore σ_o^2 when

$$\sigma_j^2 > 10\sigma_o^2 . \tag{4.40}$$

Given this, when $\text{SNR} = 20\,\text{dB}$

$$\text{SNR} = \frac{a_c^2}{\sigma_o^2} = 20\,\text{dB} = 100 \tag{4.41}$$

and

$$\sigma_o^2 = \frac{a_c^2}{100} \tag{4.42}$$

which corresponds to

$$\sigma_j^2 > 10\frac{a_c^2}{100} = \frac{a_c^2}{10}. \tag{4.43}$$

This gives us

$$\frac{a_c^2}{\sigma_j^2} = \text{SIR} < 10\,\text{dB} \tag{4.44}$$

as the range over which our results are valid when $\text{SNR} = 20\,\text{dB}$. By the same token, when $\text{SNR} = 30\,\text{dB}$, the corresponding threshold of SIR is 20 dB. These two values are the ones used in the following figures.

First of all, in Figure 30 we can see the case for $\mathrm{SNR} = 20\,\mathrm{dB}$ with code rate $r = 1/2$. The dominant characteristic is the effect of the fading upon the jamming signal. We have plotted the performance for different values of m_j including the unfaded case. We easily conclude that fading of the jamming signal works in favor of the communication system. Examining the two extremes ($m_j = 1/2$ and no fading), we observe a difference in the performance that increases as the signal-to-interference ratio decreases. As an illustration of this, for large SIR the unfaded case needs 1.8 dB more in order to achieve the same bit error rate, while for smaller values of SIR this difference is doubled.

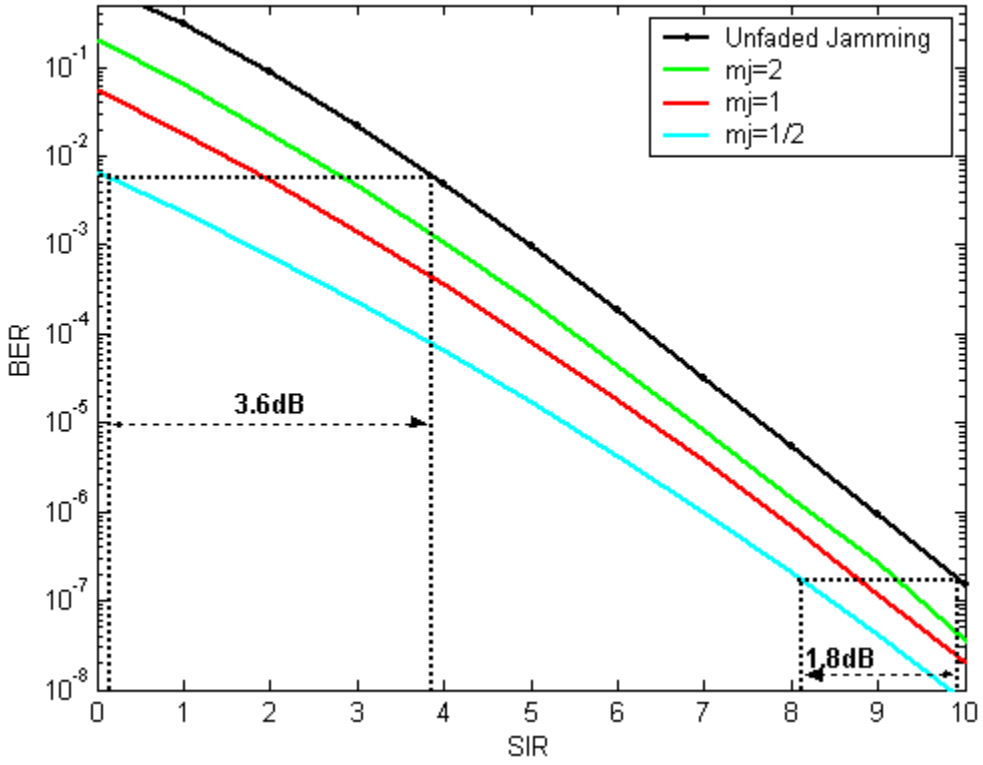

Figure 30. Performance of BPSK/QPSK with FEC and SDD for $m_s = 1$, $\mathrm{SNR} = 20\,\mathrm{dB}$, and $r = 1/2$.

In Figure 31 we see more or less the same picture. An interesting point is revealed when looking closer at the variation of m_j. The m_j parameter is allowed to vary from one half to infinity, and those two extremes produce different results. We observe that an increase of m_j produces a disproportional deterioration in performance. To make this

clear, we will look at the SIR required to achieve a specific bit error rate. The minimum SIR required for $P_b = 10^{-4}$ is 3.6 dB and is achieved for $m_j = 1/2$. The corresponding maximum value of SIR for the same P_b occurs for $m \to \infty$ and is 6.2 dB. Table 4 gives a perspective regarding different changes in m_j and the corresponding decrease in performance. From the first column, for m_j increasing from $1/2$ to 1, we need 1.2 dB more to get $P_b = 10^{-4}$. After a further increase of one more unit, $m_j = 1 \to 2$, we need another1.9 dB. From that point and on ($m_j = 2 \to \infty$), which is a vast change, we need only

Table 4. Performance difference (dB) between different m_j for $P_b = 10^{-4}$.

Change of m_j	$m_j = 1/2 \to 1$	$m_j = 1 \to 2$	$m_j = 2 \to \infty$
Decrease in performance	1.2 dB	1.9 dB	2.7 dB

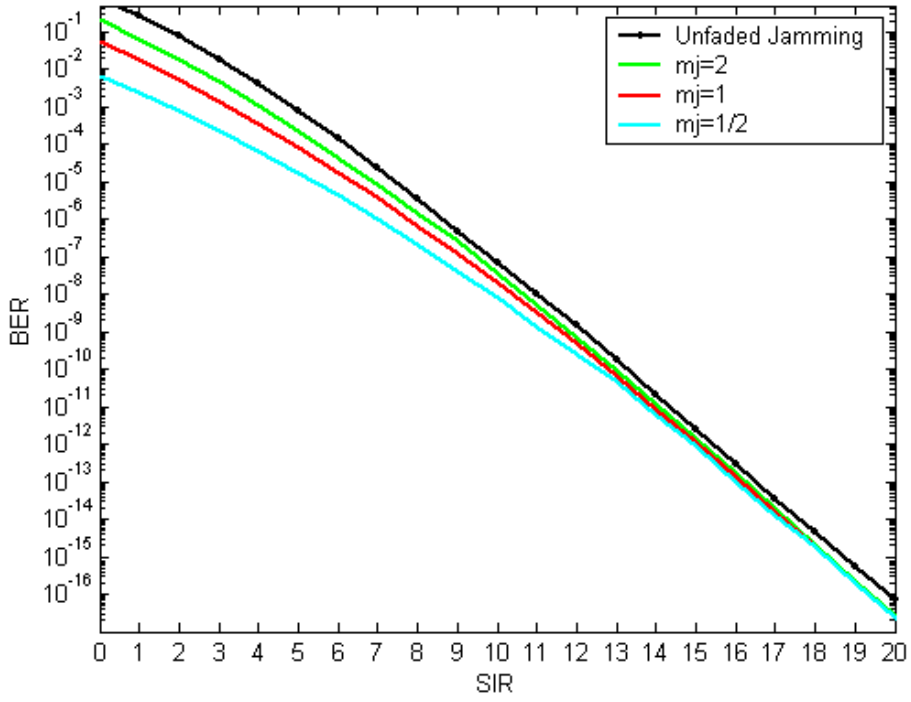

Figure 31. Performance of BPSK/QPSK with FEC and SDD for $m_s = 1$, SNR = 30 dB, and $r = 1/2$.

2.2 dB, a comparatively small change. From this we can conclude that $m_j > 2$ rapidly approaches the non-faded case.

In Figure 32 we overlay the results of the two previous figures for $\mathrm{SNR} = 20\,\mathrm{dB}$ and $\mathrm{SNR} = 30\,\mathrm{dB}$ to make it easier to compare the two. For the range of SIR we examine, the change of SNR does not affect the bit error rate when the jamming signal is faded. When the jamming signal is unfaded, the $\mathrm{SNR} = 30\,\mathrm{dB}$ case performs slightly better for large SIR.

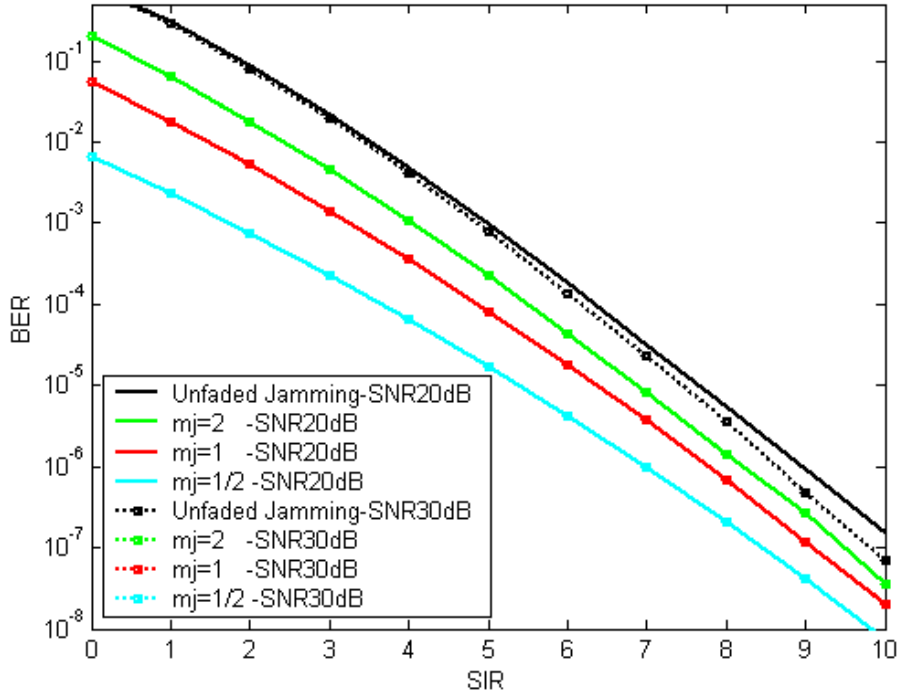

Figure 32. Comparison of BPSK/QPSK with FEC and SDD for $m_s = 1$, and $r = 1/2$.

Now, we examine differences that are introduced by changes in the code rate. For $r = 3/4$ the system achieves data rates of nine Mbps for BPSK and 18 Mbps for QPSK. We plot the results in Figures 33 and 34 for signal-to-noise ratios of 20 dB and 30 dB, respectively. Not surprisingly, the overall performance is degraded. This is the toll paid for the higher data rates. Other than this, the previous comments remain valid.

A final remark results from Figure 31 and 34. In both of them, for $\mathrm{SIR} > 16\,\mathrm{dB}$ we get the impression that the curves for the faded jamming signal do not converge with the one for the unfaded case, which is the expected result. We attribute this discrepancy to

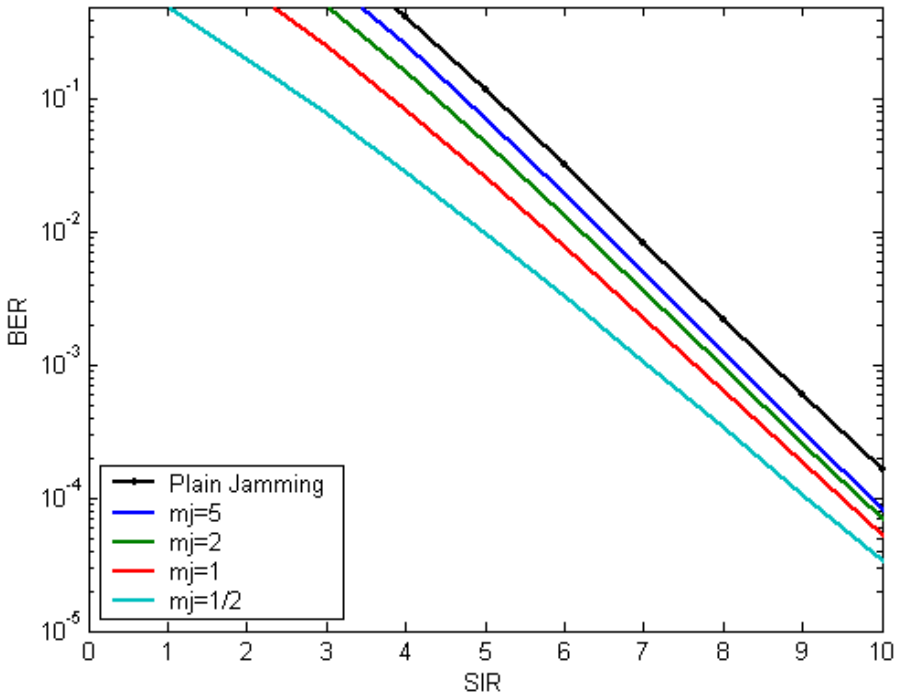

Figure 33. Performance of BPSK/QPSK with FEC and SDD for $m_s = 1$, SNR $= 20$ dB, and $r = 3/4$.

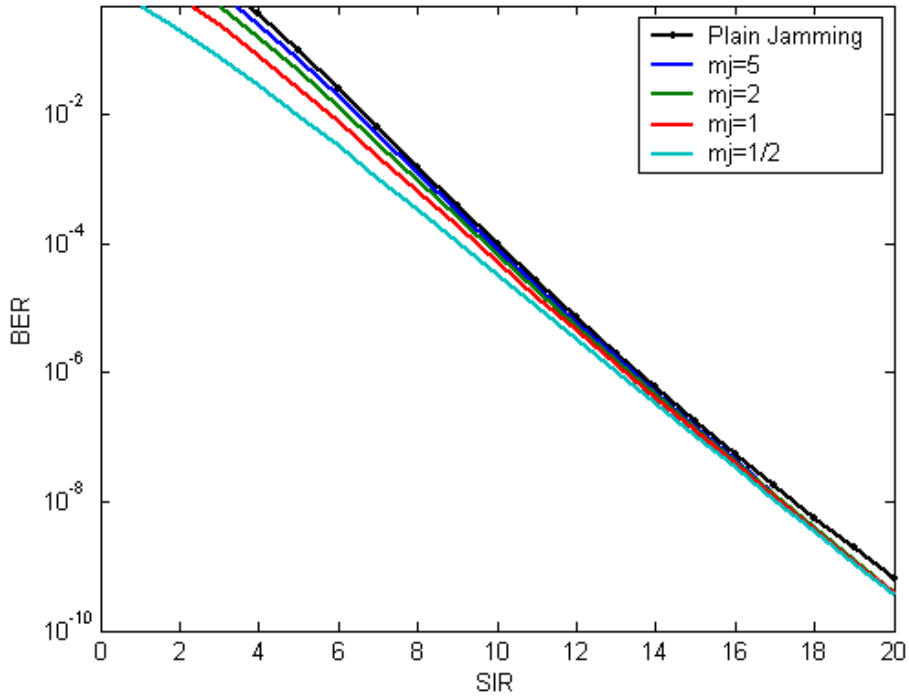

Figure 34. Performance of BPSK/QPSK with FEC and SDD for $m_s = 1$, SNR $= 30$ dB, and $r = 3/4$.

the assumption that SNR is large. As explained, when SIR is large, the validity of the assumption is marginal and that is the reason the curves do not converge to the unfaded case as m_j increases for large SIR.

3. Comparison of BPSK/QPSK with and without FEC and SDD

We can now make a comparison between coded and uncoded BPSK/QPSK in order to determine coding gain. In Figures 35 and 36 we present the performance for $\text{SNR} = 30\,\text{dB}$ with $r = 1/2$ and $r = 3/4$, respectively. There is an obvious advantage in favor of FEC with SDD. Rayleigh fading of the information signal, as has already been mentioned, prevents uncoded BPSK from achieving a small enough probability of bit error for reasonable SNR. Even for $\text{SNR} = 30\,\text{dB}$ and $\text{SNR} = 20\,\text{dB}$, P_b is no smaller than 10^{-3}. The performance is so bad that whatever the benefit from the faded jamming signal, P_b is too large. These plots depict the problems when an uncoded signal is subject to severe fading. Communication in such an environment is unattainable. That is the reason

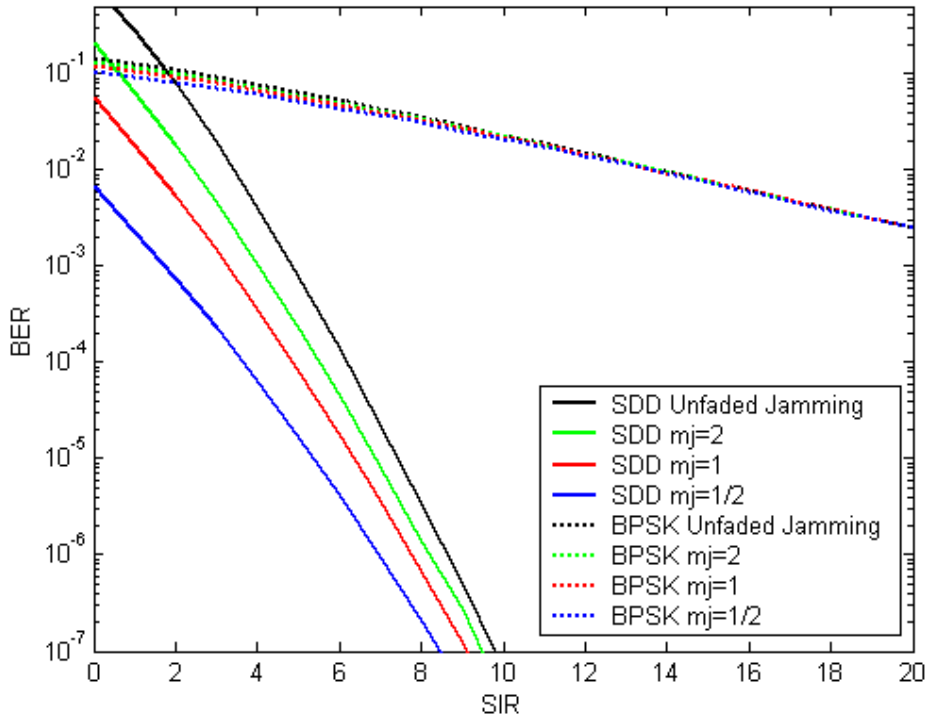

Figure 35. Comparison of coded and uncoded BPSK/QPSK for $m_s = 1$, $\text{SNR} = 30\,\text{dB}$, and $r = 1/2$.

the IEEE 802.11a waveform exploits forward error correction coding. The improvement is such as to effectively overcome the effects of fading.

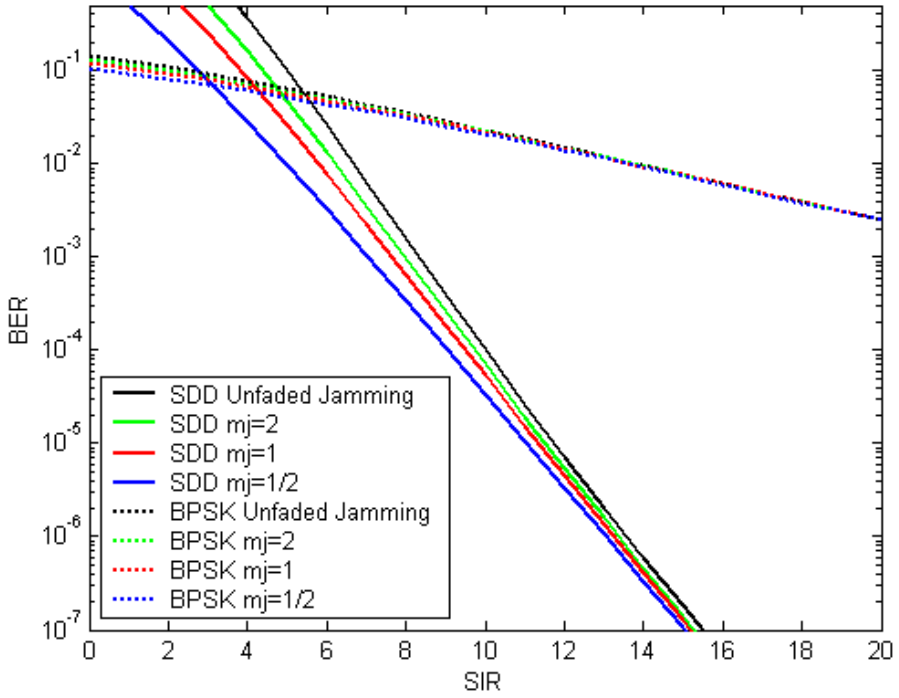

Figure 36. Comparison of coded and uncoded BPSK/QPSK for $m_s = 1$, SNR = 30 dB, and $r = 3/4$.

C. 16QAM/64QAM

MQAM is used by IEEE 802.11a to achieve the highest data rates the standard offers, from 24 Mbps (16QAM, $r = 1/2$) to 54 Mbps (64QAM, $r = 3/4$). The analysis is similar to that for BPSK with the difference of the initial expression for P_b in AWGN plus jamming:

$$P_{b_{MQAM}} = \frac{4(M-1)}{q\sqrt{M}} Q\left(\sqrt{\frac{3q}{M-1} \cdot \frac{a_c^2}{\sigma_j^2 + \sigma_o^2}}\right) \tag{4.45}$$

As we have explained previously, we neglect σ_o^2 to facilitate our analysis. Recalling the definition of the ratio a_c^2 / σ_j^2 in Equation (4.3) as the random variable t, the probability of bit error is written as

$$P_{b_{MQAM}}(t) = \frac{4(M-1)}{q\sqrt{M}} Q\left(\sqrt{\frac{3q}{M-1}t}\right) \tag{4.46}$$

and is conditional on t. Lastly, using the pdf of t from Equation (4.15), we can evaluate Equation (4.16) numerically.

In Figures 37, 38 and 39, we see the resulting plots for uncoded 16QAM where m_s has the values of 1/2, 1, and 2, respectively. The findings are similar to the ones obtained for BPSK. The signal experiencing Rayleigh fading is the only case where the curves for all m_j converge. The primary difference from BPSK is the overall poorer performance, which is expected. To complete the discussion, we examine the last modulation (64QAM) in Figure 40. Its characteristics are analogous to those obtained for 16QAM and have already been explained.

The expansion of uncoded MQAM to MQAM with FEC and SDD seems straightforward. Small alterations are required in the expressions previously obtained for FEC with SDD. However, limitations of the software used lead to significant numerical difficulties, so the analysis of MQAM with FEC and SDD is not pursued here.

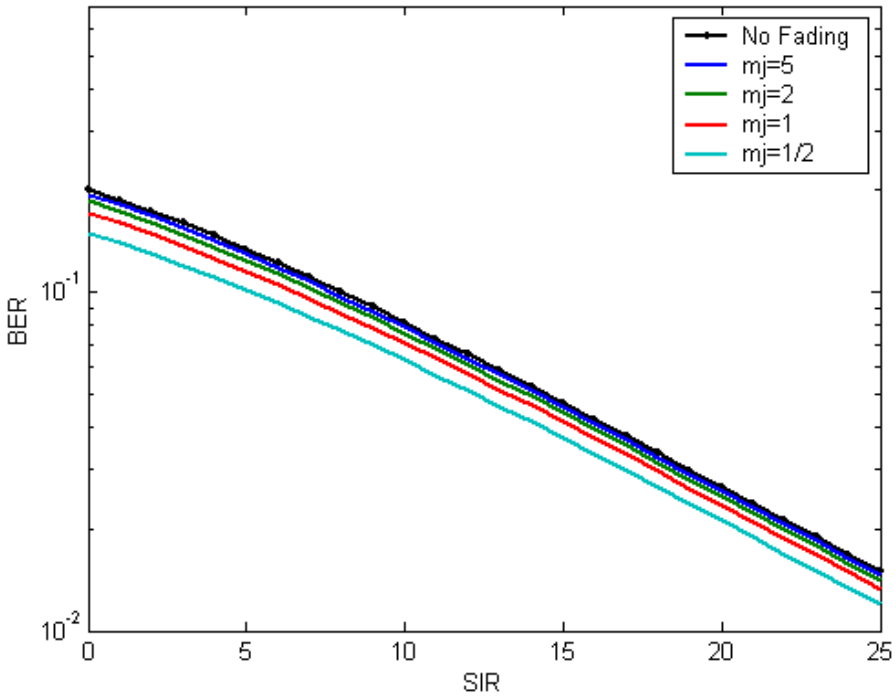

Figure 37. Performance of 16QAM ($m_s = 1/2$).

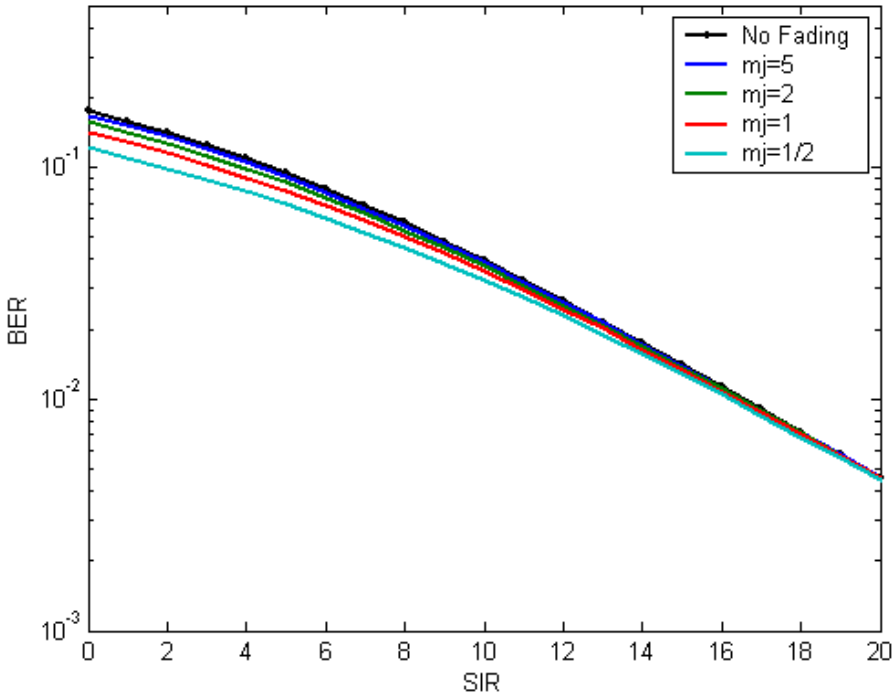

Figure 38. Performance of 16QAM ($m_s = 1$).

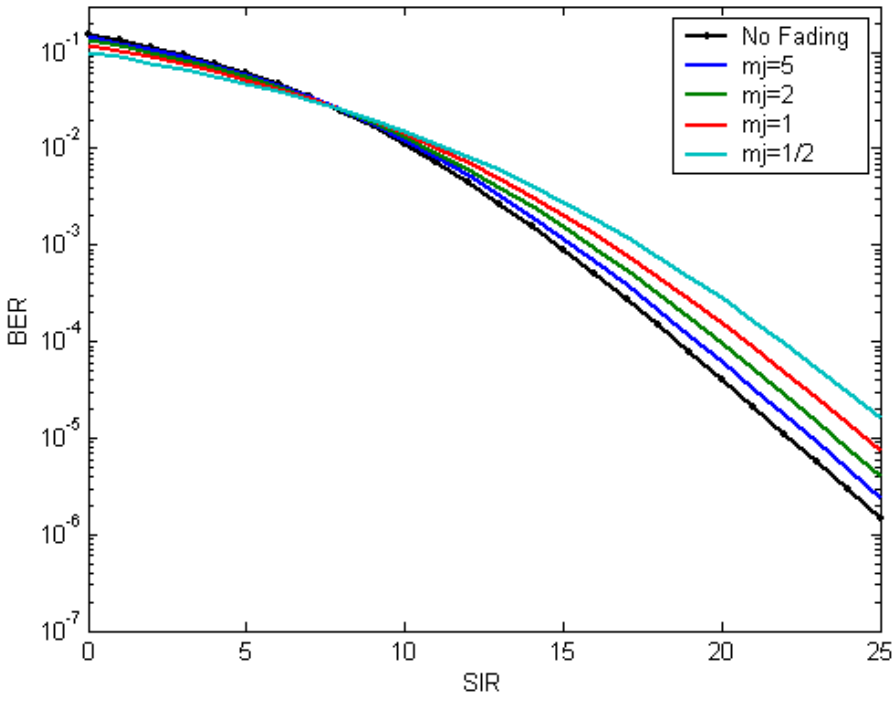

Figure 39. Performance of 16QAM ($m_s = 3$).

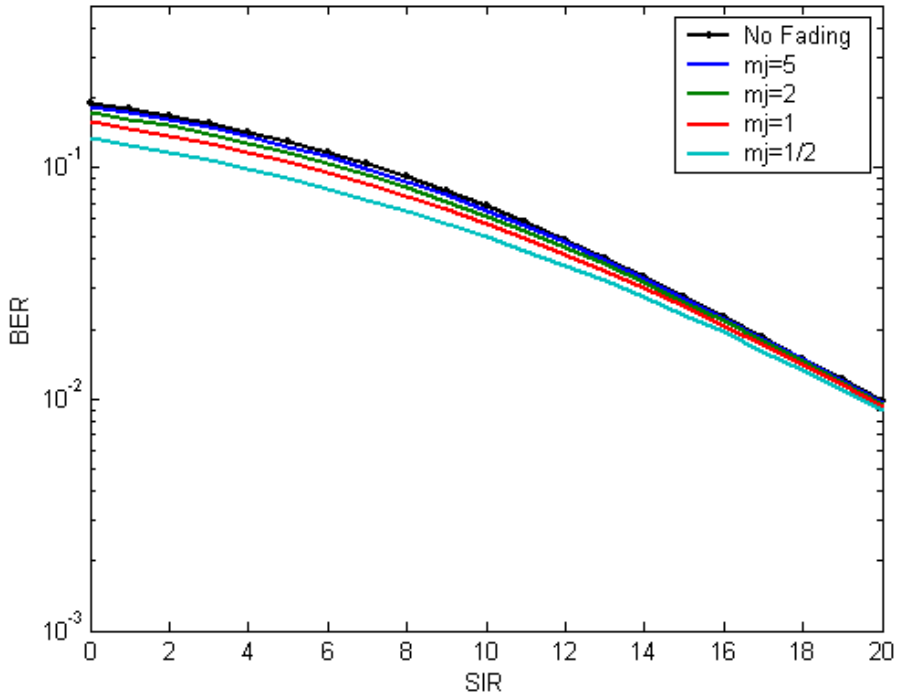

Figure 40. Performance of 64QAM ($m_s = 1$).

D. SUMMARY OF FADED JAMMING

Summarizing the analysis of this chapter, we investigated all modulations that the IEEE 802.11a waveform exploits. We followed the structure of the third chapter and, initially, we investigated the performance of BPSK/QPSK. The great milestone in the analysis was the derivation of Equation (4.15), which enabled us to deal with the conditional probability of bit error and to derive the necessary expressions for the faded jamming signal. To be consistent with our initial assumption, we recollect that the results are valid for large values of SNR. A surprising finding was that the fading conditions of the jamming signal are not enough to determine the effect upon the performance of our communication system. The fading conditions of the desired signal are necessary as well. We found that for $m_s \le 1$, fading of the jamming signal improves bit error rate. On the other hand, when $m_s > 1$ the previous statement is valid only for small SIR, as indicated by Table 3. For larger values of SIR, the performance deteriorates for increasingly severe fading of the jamming waveform.

Continuing, we narrowed the possible signal fading conditions to Rayleigh due to practical difficulties encountered in the numerical evaluation required for FEC with SDD. Thus, we derived Equation (4.39), which is the core of the chapter concerning coded performance. Although it is expressed in the Laplace domain, the use of the numerical inverse of the two-sided Laplace transformation from [9] easily overcame that difficulty. The resulting plots reinforced the validity of the findings for uncoded BPSK for the $m_j = 1$ case. Moreover, it became apparent that FEC with SDD is essential when there is severe signal fading, since FEC with SDD tremendously improves the bit error rate.

THIS PAGE INTENTIONALLY LEFT BLANK

V. CONCLUSION

A. INTRODUCTION

The goal of this thesis was to investigate the performance of WLAN systems. Due to its popularity and its high data rates, we selected IEEE 802.11a standard as a representative standard. Using the actual characteristics of the standard, we investigated all modulation types the standard specifies. Additionally, we examined the informational signal with and without FEC with SDD.

In every case we studied, the effect of fading and pulsed-noise jamming was considered. The study of FEC with SDD revealed significant results that support the use of error correction to mitigate effects of fading. Then we incorporated into the analysis the effect of the fading channel on the jamming signal to obtain a realistic estimate of the effect of hostile jamming when the information signal is transmitted over a fading channel.

B. FINDINGS

We began the analysis in Chapter III, where the fading channel was assumed to affect only the informational signal. The result was that performance for a signal with FEC and SDD and for a signal without coding exhibits the same characteristics; as m_s increases, performance improves. Examining the optimum strategy for pulsed-noise jamming, we tested different values of p. We found that continuous jamming is most effective when the receiver employs coding in all fading environments.

In Chapter IV we introduced fading of the jamming signal. Without FEC with SDD, fading of the jamming signal decreased the probability of bit error for all modulation types when $m_s \leq 1$. For larger values of m_s and for small SIR, the probability of bit error was again decreased as the fading of the jamming signal became more severe. The opposite behavior was seen when SIR was increased, when performance deteriorated.

Based on the finding that the worst-case for signals with FEC and SDD is continuous jamming, we used $p = 1$ for the analysis in the second part of Chapter IV, where the signal employed FEC with SDD. The cases of fading of the desired signal we studied

were limited to Rayleigh due to extreme complexity of the calculations when $m_s \neq 1$. In this case a decrease of m_j improves performance.

C. RECOMMENDATIONS FOR FURTHER RESEARCH

Although this thesis focuses on IEEE 802.11a signals, the findings can be used in a broad field of communication systems. Every system utilizing either MPSK or MQAM with FEC with SDD and pulsed-noise jamming can be examined using our analysis. Small alterations regarding the code rate and the encoder are enough to find the performance of other standards. The same is true as regards the study of the effect of fading on the jamming signal. Additionally, the approach followed can be exploited even when investigating MFSK modulation.

Our results are heavily based on numerical evaluations. If the analysis can be taken further analytically, some of the numerical difficulties encountered here might be avoided. The generation of plots for the cases we did not pursue might be feasible, like the performance for modulations other than BPSK/QPSK when the jamming signal experiences fading and the fading of the desired signal is other than Rayleigh.

The methodology of the numerical inverse of the two-sided Laplace transform from [9] was a key point. Numerical evaluation would not be realizable without its use in Chapters III and IV. It is the pillar of this work and will be useful to anyone facing problems of this nature. Nonetheless, additional research might focus on techniques to minimize numerical problems that are sometimes encountered using this methodology.

Regarding OFDM, further research could investigate different options for the distribution of m. We arbitrary assumed m to be uniformly distributed, and we ranged its value from one half to five. More accurate results would be produced by a study with field measurements to determine the actual range of m.

D. CLOSING COMMENTS

WLANs are increasingly important in meeting the demand for high data rates. FEC with SDD and OFDM offer the potential to mitigate fading effects and achieve sub-

stantial performance improvement. Their analysis is essential, since WLANs enjoy acceptance from the broadband wireless communications systems of the next generation.

THIS PAGE INTENTIONALLY LEFT BLANK

LIST OF REFERENCES

1. L. Wan and V.K. Dubey, "Bit Error Probability of OFDM Systems Over Frequency-nonselective Fast Rayleigh Fading Channels," *IEE Electronics Letters*, vol. 36, pp. 1306-07, July 2000.

2. L. Wan and V.K. Dubey , "BER Probability of OFDM Systems Over Frequency-nonselective Fast Ricean Fading Channels," *IEE Electronics Letters*, vol. 5, pp. 19-21, January 2001.

3. Count A. Patrick, "Performance Analysis of OFDM Frequency-Selective, Slowly Fading Nakagami Channels," Master's Thesis, Naval Postgraduate School, Monterey, California, 2001.

4. Irfan Kosa, "Performance of IEEE 802.11a Wireless LAN Standard over Frequency-Selective, Slowly Fading Nakagami Channels in a Pulsed Jamming Environment," Master's Thesis, Naval Postgraduate School, Monterey, California, 2002.

5. John D. Oetting, "The Effects of Fading on Antijam Performance Requirements," *IEEE Journal on Selected Areas in Communications*, vol. SAC-5, no. 2, pp. 155-161, February 1987.

6. A. H. Wojnar, "Unknown Bounds on Performance in Nakagami Channels," *IEEE Trans. Commun.*, vol. COM-34, pp. 22-24, January 1986.

7. Bruce McGuffin, "Jammed FH-FSK Performance in Rayleigh and Nakagami-m Fading," *Proc. of MILCOM* 2003.

8. Minoru Nakagami, "The m-Distribution – A General Formula of Intensity Distribution of Rapid Fading," in *Statistical Methods in Radio Wave Propagation*, W. C. Hoffman (ed.), pp. 3-36, Pergamon Press, New York, 1960.

9. Clark Robertson, Notes for EC4550 (Digital Communications)**,** Naval Postgraduate School, Monterey, California, 2003 (unpublished).

10. Institute of Electrical and Electronics Engineers, *802.11a, Wireless LAN Medium Access Control (MAC) and Physical Layer (PHY) Specifications: High-Speed Physical Layer Extension in the 5 GHz Band,* 16 September 1999.

11. B. Sklar, *Digital Communications: Fundamental and Applications*, 2nd ed., Prentice Hall, Upper Saddle River, New Jersey, 2002.

12. Clark Robertson, Notes for EC4580 (Coding and Information)**,** Naval Postgraduate School, Monterey, California, 2001 (unpublished).

13. Theodore S. Rappaport, *Wireless Communications Principles and Practice*, 2nd ed., Prentice Hall, Upper Saddle River, New Jersey, 2002.

14. J.G. Proakis, *Digital Communications,* 4th ed., McGraw Hill, New York, 2001.

15. A. Papoulis, *Probability, Random Variables, and Stochastic Processes*, 3nd ed., McGraw Hill, New York, 1991.

16. I.S. Gradshteyn and I.M. Ryzhik, *Tables of Integrals, Series, and Products,* Academic Press, New York, 1980.

INITIAL DISTRIBUTION LIST

1. Defense Technical Information Center
   Ft. Belvoir, Virginia

2. Dudley Knox Library
   Naval Postgraduate School
   Monterey, California

3. Chairman, Code EC/Po
   Department of Electrical and Computer Engineering
   Naval Postgraduate School
   Monterey, California

4. Chairman, Code SM/Bo
   Department of Information Science
   Naval Postgraduate School
   Monterey, California

5. Professor R. Clark Robertson EC/Rc
   Department of Electrical and Computer Engineering
   Naval Postgraduate School
   Monterey, California

6. Professor Donald van Zelm Wadsworth EC/Wd
   Department of Electrical and Computer Engineering
   & Space Systems Academic Group
   Naval Postgraduate School
   Monterey, California

7. Embassy of Greece Office of Naval Attache
   Washington, DC

8. 18 Anakreontos st.
   Andreas Tsoumanis
   Egaleo-Athens, Greece 12243